Redox Biology 78 (2024) 103353

Contents lists available at ScienceDirect

Redox Biology

journal homepage: www.elsevier.com/locate/redox

Role of Hippo/ACSL4 axis in ferroptosis-induced pericyte loss and vascular dysfunction in sepsis

Yiyan Liu [a,1], Daiqin Bao [b,1], Han She [b,1], Zisen Zhang [a], Shifeng Shao [c], Zhengbin Wu [c], Yue Wu [a], Qinghui Li [a], Li Wang [a,*], Tao Li [a,**], Liangming Liu [a,***]

[a] Shock and Transfusion Department, Daping Hospital, Army Medical University, Chongqing, 400042, China
[b] Department of Anesthesiology, Daping Hospital, Army Medical University, Chongqing, 400042, China
[c] Department of Critical Care Medicine, Daping Hospital, Army Medical University, Chongqing, 400042, China

ARTICLE INFO

Keywords:
Sepsis
Ferroptosis
Pericyte loss
ACSL4
Vascular permeability
Hippo pathway

ABSTRACT

Sepsis is a critical condition characterized by a systemic inflammatory response to infection, often leading to severe vascular dysfunction and high mortality. One of the hallmarks of vascular dysfunction in sepsis is increased vascular permeability and the loss of pericytes, which are essential for maintaining vascular integrity. Despite the significance of pericyte loss in sepsis, the primary type of cell death responsible and the underlying molecular mechanisms remain incompletely understood. This study aims to elucidate these mechanisms by focusing on ferroptosis, a form of programmed cell death, and its regulation through the Hippo/ACSL4 axis. Our research confirmed significant pericyte loss in patients with sepsis. Through advanced single-cell analysis and proteomics, ferroptosis was identified as a key differentiating cell death type between sepsis and sham samples. Further metabolomics analysis revealed that Acyl-CoA Synthetase Long-Chain Family Member 4 (ACSL4) plays a pivotal role in the ferroptosis of pericytes during sepsis. In vitro experiments demonstrated that downregulation of ACSL4 effectively reduced lipopolysaccharide (LPS)-induced lipid peroxidation, restored pericyte viability, and improved endothelial permeability. In vivo studies with pericyte-specific ACSL4 knockout mice showed a marked decrease in pericyte loss and enhanced vascular barrier function following sepsis induction. To translate these findings into potential therapeutic strategies, we developed pericyte-targeting liposomes encapsulating ACSL4 shRNA adenovirus. These liposomes successfully restored pulmonary vascular barrier function and significantly reduced pericyte loss in septic conditions. The results of this study underscore the crucial role of ACSL4 in mediating ferroptosis in pericytes and highlight the therapeutic potential of targeting ACSL4 to mitigate vascular dysfunction in sepsis.

1. Introduction

Sepsis is a systemic, dysregulated host response to infection that can rapidly progress to fatal organ dysfunction. The mortality rate for sepsis ranges from 30 % to 35 % [1]. The Third International Consensus Definitions for Sepsis and Septic Shock (Sepsis-3) highlight that profound circulatory, cellular, and metabolic abnormalities significantly increase mortality risk [2]. Vascular dysfunction is a critical component in the pathophysiology of multiple organ dysfunction syndrome (MODS) that follows sepsis [3–5]. Thus, a comprehensive exploration of the underlying mechanisms of vascular dysfunction and developing novel therapeutic strategies is imperative.

Pericytes are microvascular mural cells that cover the largest capillary surface area, from precapillary arterioles to postcapillary venules

* Corresponding author. Shock and Transfusion Department, Daping Hospital, Army Medical University, No.10, Changjiang Road, Yuzhong District, Chongqing, 400042, China.
** Corresponding author. Shock and Transfusion Department, Daping Hospital, Army Medical University, No.10, Changjiang Road, Yuzhong District, Chongqing, 400042, China.
*** Corresponding author. Shock and Transfusion Department, Daping Hospital, Army Medical University, No.10, Changjiang Road, Yuzhong District, Chongqing, 400042, China.
E-mail addresses: wangli123@tmmu.edu.cn (L. Wang), lt200132@tmmu.edu.cn (T. Li), lmliu62@tmmu.edu.cn (L. Liu).
[1] These authors contributed equally to this work.

https://doi.org/10.1016/j.redox.2024.103353
Received 24 June 2024; Received in revised form 27 August 2024; Accepted 11 September 2024
Available online 12 November 2024

[6–8]. They are crucial in regulating blood flow, supporting vessel walls, and maintaining vascular barrier integrity [9,10]. Previous studies have demonstrated that pericyte loss is closely associated with vascular barrier dysfunction and hyporeactivity following sepsis. Moreover, the infusion of cultured pericytes has been shown to protect against sepsis by homing, colonizing, and secreting microvesicles [11–13]. However, the precise mechanisms underlying pericyte dysfunction and loss in sepsis remain unclear.

Nish et al. identified that the impairment of the Sirt3/angiopoietins/Tie-2 pathway and the HIF-2α/Notch3 pathway was critical for lung pericyte loss following sepsis [14]. Furthermore, Hongkuan Fan et al. demonstrated that knockout of Fli-1 in pericytes attenuated lung pericyte loss and vascular leak, thereby reducing the mortality of septic mice [15–17]. This loss was unrelated to apoptosis, prompting further investigation into the types of programmed cell death involved in pericyte damage during sepsis.

Ferroptosis is a new type of iron-dependent programmed cell death and highly rely on reactive oxygen species (ROS) availability [18]. Ferroptosis occurs to cells when polyunsaturated fatty acids (PUFAs)--containing phospholipids (PLs) interact with intracellular ROS, which is called lipid peroxidation [18]. Recent studies have showed that ferroptosis has been implicated in the pathogenesis of several diseases, including infectious diseases, cancer and ischemic organ injury [19]. Furthermore, ferroptosis plays a crucial role in multiple organ dysfunction in sepsis [20]. Zhang et al. have demonstrated that dexmedetomidine alleviated sepsis-induced heart injury via inhibiting ferroptosis [21]. Li et al. have demonstrated that irisin protects against sepsis-associated encephalopathy by suppressing ferroptosis via activation of the Nrf2/GPX4 signal axis [22]. Given this association, targeting ferroptosis emerge as a promising strategy for treating sepsis-induced organ dysfunction.

PUFAs-PLs complexes are generated by cells via Acyl-CoA Synthetase Long-Chain Family Member 4 (ACSL4) which ligate free PUFAs with CoA to produce PUFAs–CoAs [23]. This process is crucial to the onset of ferroptosis. To keep redox balance, cells have developed antioxidant systems to clear and neutralize lipid peroxidation and to prevent ferroptosis. The glutamine peroxidase 4 (GPX4)-glutamine (GSH) system is the most famous [24]. GPX4 with its cofactor GSH, can reduce peroxidation. Numerous genetic and nongenetic factors can both regulate and determine ferroptosis. Recent studies have pointed out that cell density can also have an important effect on ferroptosis [25,26]. Simply put, the lower the tumor density, the higher the sensitivity to ferroptosis. In this process, The Hippo pathway counts a lot. As mesothelioma cell density increased, the expression of E-cadherin was increased and further activated the NF2–Hippo axis, which suppressed YAP and ferroptosis. Experimental disruption of the NF2–Hippo axis in mesothelioma cell lines activated YAP, which enhanced cellular sensitivity to ferroptosis.

This study aims to investigate the specific mechanisms of pericyte damage in sepsis. Using proteomics, we found that the expression of ACSL4 on pericytes was significantly elevated in sepsis. Conditional knockout of ACSL4 in pericytes significantly reduced the mortality of septic mice by preventing pericyte loss and preserving vascular barrier function. Furthermore, we propose that pericyte-targeting liposomes encapsulating ACSL4-shRNA adenovirus could be a novel therapeutic strategy for treating vascular dysfunction in sepsis.

2. Results

2.1. Pericyte loss and pulmonary vascular leakage in sepsis

Pericytes are perivascular cells that play a crucial role in maintaining the vascular barrier through interactions with endothelial cells [26,27]. Dysfunction and loss of pericytes contribute significantly to the pathogenesis of various diseases [28,29]. In this study, we observed that pericyte loss was closely associated with pulmonary vascular leakage in septic rats. We first established a sepsis model in rats via cecal ligation and puncture (CLP) and observed significant extravasation of FITC-BSA and Evans blue from pulmonary vessels, indicating severe impairment of pulmonary vascular barrier function in sepsis (Fig. 1A–B, Supplementary data 1A). Electron microscopy revealed disruptions in the continuity and integrity of the vascular endothelial cells in the lungs (Fig. 1C). The wet-dry ratio of the lungs and arterial blood gas indices also demonstrated severe lung function impairment in sepsis (Supplementary data 1B,1C).

To further investigate pericyte loss, we collected peripheral blood samples from sepsis patients to quantify the number of detached pericytes. This study included 30 sepsis patients and 15 healthy volunteers. Patients with sepsis exhibited significantly higher body temperatures, heart rates, and white blood cell counts than healthy controls (Fig. 1D). The number of detached pericytes in the peripheral blood of sepsis patients was significantly higher than in healthy controls (Fig. 1E), indicating substantial pericyte detachment from vascular walls during sepsis. We also examined the lung tissues of rats and confirmed pericyte loss through immunostaining and western blotting. Immunostaining showed a significant decrease in the expression of the pericyte marker NG2 in the pulmonary vascular networks of septic rats (Fig. 1F). Western blot analysis further confirmed the decreased expression of pericyte markers NG2 and PDGFR-β (Fig. 1G). These findings demonstrate that pericyte loss is closely associated with pulmonary vascular leakage in sepsis.

2.2. Ferroptosis occurred in pericytes during sepsis and inhibition of ferroptosis ameliorated pericyte loss and pulmonary vascular barrier dysfunction

Embedded in the vascular basement membrane, pericytes are essential for regulating blood flow and maintaining vascular barrier function. Our previous findings indicated a close relationship between sepsis pericyte loss and pulmonary vascular leakage [11]. Understanding the precise mechanisms behind pericyte loss and targeting pericyte treatment is crucial for developing therapies for vascular barrier dysfunction in sepsis. However, pericyte damage's transcriptomic and signaling heterogeneity during sepsis pathology remains poorly understood. Here, we combined single-cell RNA sequencing analysis in vivo with proteomics and metabolomics in vitro to investigate the specific mechanisms of pericyte impairment in sepsis.

Single-cell RNA sequencing analysis of sorted pericytes revealed that among various types of programmed cell death (PCD), including autophagy, apoptosis, ferroptosis, necroptosis, and pyroptosis, ferroptosis had the highest U-cell score (Fig. 2A). KEGG enrichment analysis of proteomics data further confirmed that the ferroptosis pathway was significantly upregulated in pericytes following the LPS challenge (Fig. 2B–C). Consequently, we treated pericytes with different PCD inhibitors and found that ferroptosis inhibitors, autophagy, and pyroptosis significantly rescued pericyte viability after the LPS challenge. Among these, Ferrostatin-1 (Fer-1) was the most effective ferroptosis inhibitor, restoring pericyte viability by 52.81 % (Fig. 2D). These results suggest that ferroptosis is a key factor in pericyte damage during sepsis.

To confirm the involvement of ferroptosis in pericyte damage, we examined the effects of Fer-1 on ferroptosis markers in pericytes post-LPS challenge. LPS stimulation led to substantial lipid peroxidation and ferrous iron accumulation in pericytes, which were significantly attenuated by Fer-1 treatment (Fig. 2E–Supplementary data 2A). Additionally, Fer-1 increased the GSH and the GSH/GSSG ratio in pericytes (Fig. 2E). We further detected the expression of GPX4 and COX2 and found that LPS stimulation led to significant elevated expression of COX2 and decreased expression of GPX4 in pericytes, which were significantly reversed by Fer-1 treatment (Supplementary data 2B). These findings indicate that severe ferroptosis occurs in pericytes following LPS stimulation and that Fer-1 significantly mitigates pericyte ferroptosis, restoring viability.

We further evaluated Fer-1's impact on the vascular endothelial cell

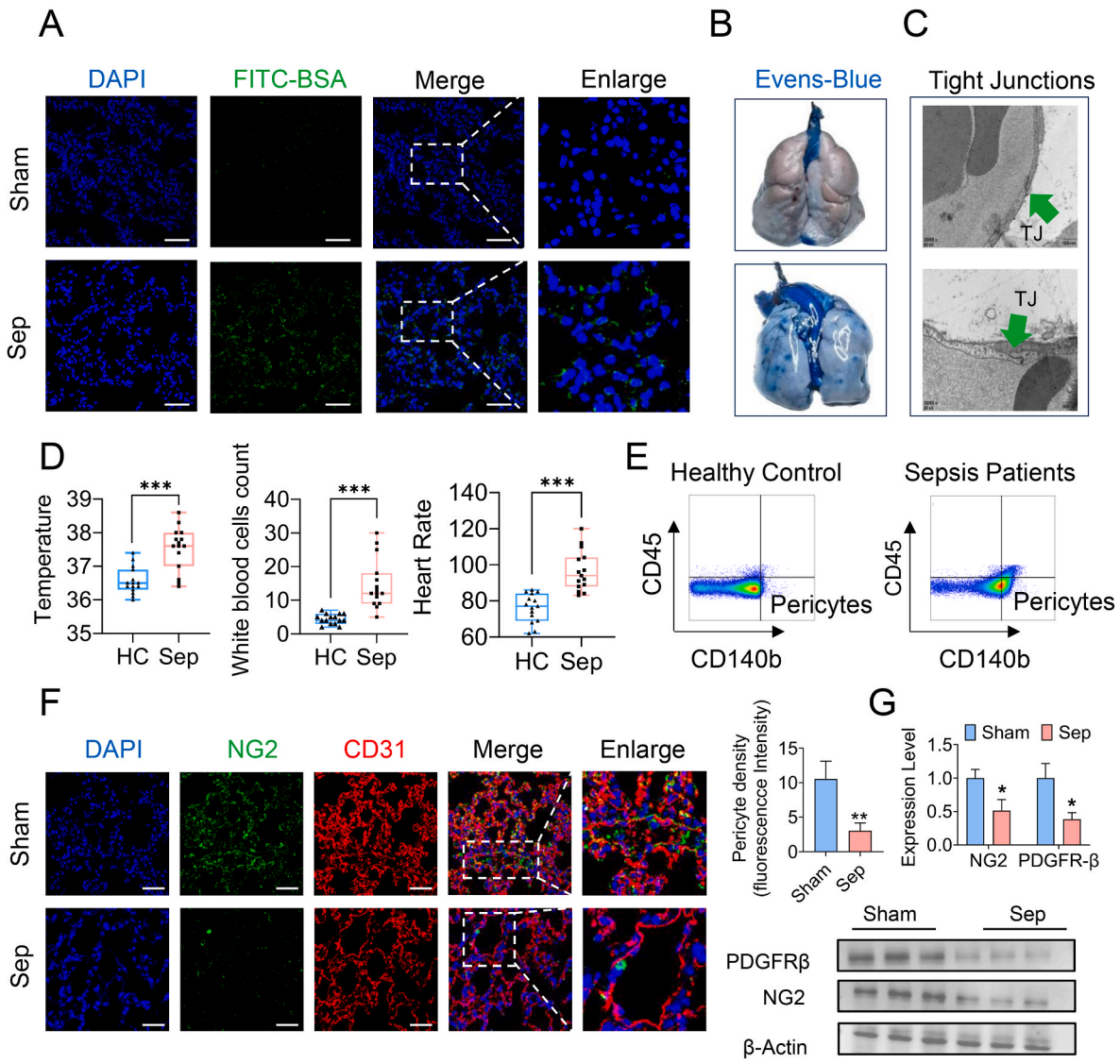

Fig. 1. Sepsis induced pericytes loss and pulmonary vascular permeability. (A) Representative images of FITC-BSA leakage in the lung tissues. (Blue, DAPI; green, FITC-BSA. Bar = 50 μm) (B) Representative images of Evens-Blue leakage in the lung tissues. (n = 6/group) (C) Representative TEM images of tight junctions in pulmonary vessels following sepsis (green arrow indicate the tight junction. Bar = 1 μm) (D) Body temperature, white blood cells count and heart rate of septic patients and healthy controls (HC). (septic patients n = 8, HC n = 8) (E) Flow cytometry analyses of $CD45^{-}CD140b^{+}$ cells (pericytes) in the serum of septic patients and healthy controls. (septic patients n = 8, HC n = 8) (F) Laser confocal microscopy analysis of the pulmonary networks. (NG2, green, pericyte marker; CD31, red, endothelial cell marker. Bar = 50 μm) (G) Western blotting analysis of pericyte marker (PDGFR-β and NG2) in the lung tissues. (n = 3/group)
Data were shown as mean ± SD. *p < 0.05, *p < 0.01, ***p < 0.001. Statistical significance was determined by two-sided Student's-test as appropriate. (For interpretation of the references to colour in this figure legend, the reader is referred to the Web version of this article.)

(VEC) barrier and found that Fer-1 administration reduced BSA-FITC leakage (Fig. 2F) and VEC TEER (Supplementary data 2C), indicating alleviated endothelial leakage.

To elucidate the role of pericyte ferroptosis in pulmonary vascular leakage during sepsis in vivo, we treated rats with Fer-1 before CLP and observed changes in pericyte ferroptosis and pulmonary vascular barrier function. Fer-1 treatment reduced the content of lipid ROS in lung tissue pericytes by 37.60 % (Fig. 2G) and significantly attenuated pericyte loss, as shown by increased expression of NG2 and PDGFR-β in western blotting (Fig. 2H–Supplementary data 3A) and immunostaining (Fig. 2I–Supplementary data 3B). Additionally, Fer-1 treatment significantly reduced the extravasation of FITC-BSA (Supplementary data 3C) and Evans blue (Fig. 2J) and improved the integrity and ultrastructure of tight junctions (Fig. 2K). Fer-1 also significantly decreased the wet-dry ratio of the lungs (Fig. 2L), improved lung histopathology (Supplementary data 3D), arterial blood gas indices (Supplementary data 3E), and reduced serum levels of IL-6 and TNF-α (Fig. 2M). These improvements translated to enhanced survival, with the Fer-1 group exhibiting a mean survival time of 57.7 h compared to 34.8 h in the sepsis group and a 72-h survival rate of 43.75 % (7/16) versus only one survivor in the sepsis group (Fig. 2N). In addition, we isolated the pulmonary veins and detected the contents of LPO (Supplementary data 4A) and the expression levels of classical molecules of ferroptosis (GPX4 and COX2) in pulmonary vein tissues (Supplementary data 4B). WB results found that the expression of COX2 was significantly elevated and the expression of GPX4 was significantly decreased in the pulmonary vein tissues following sepsis. Fer-1 pretreatment restored the expression of GPX4 and decreased the expression of COX2. A large amount of lipid peroxides was generated in the pulmonary vein tissues following sepsis and the content of LPO in the Fer-1 pretreatment group was 47.09 % lower than that in the Sep group.

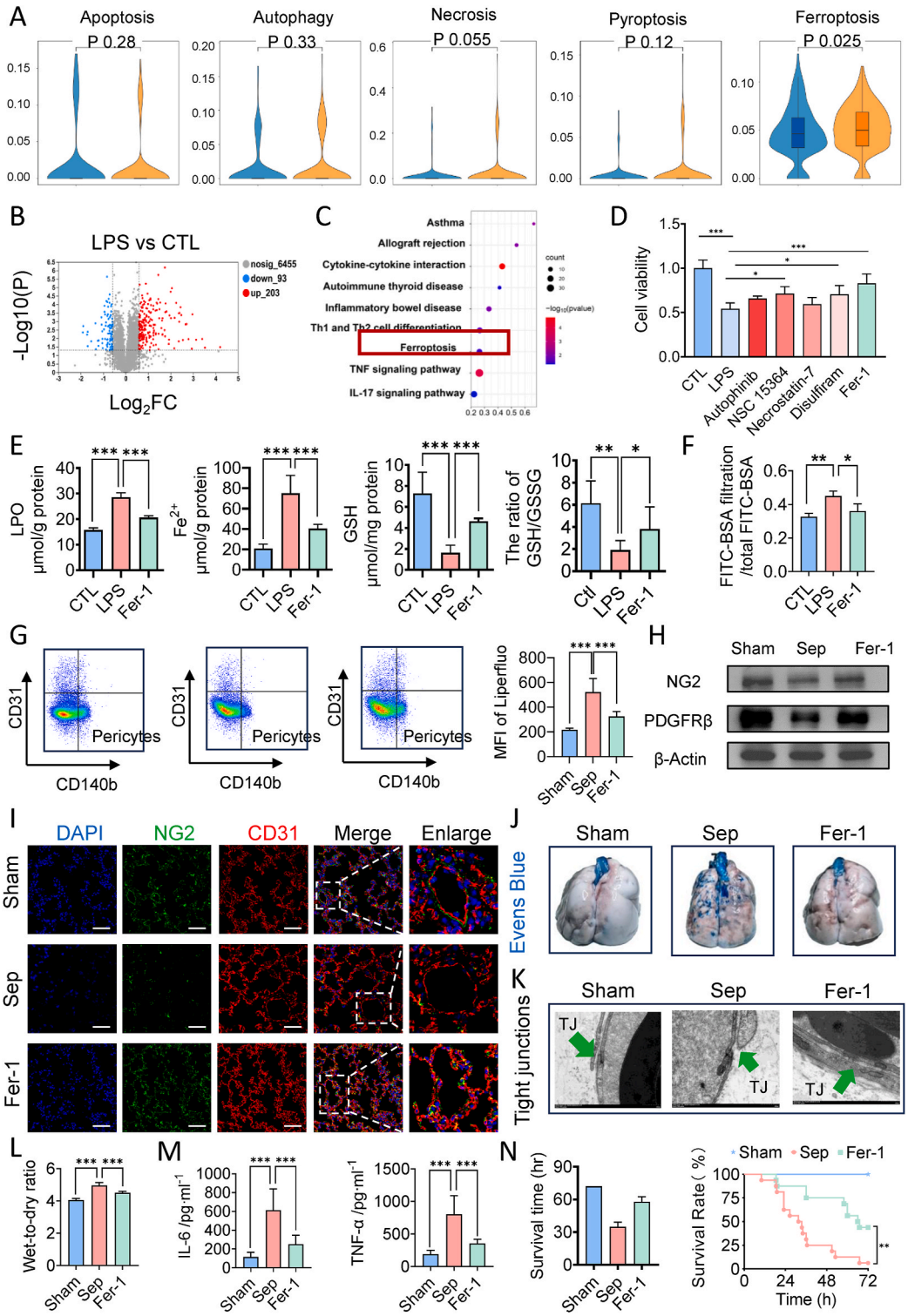

Fig. 2. Pericyte underwent ferroptosis and inhibition of ferroptosis alleviated sepsis-related pulmonary vascular leakage. (A) U-cell score of different programmed cell death (PCD) of pericytes in mice following sepsis. (B) Volcano plot of differentially expressed genes between control groups and LPS treated groups. (C) KEGG pathway (upregulated) of differentially expressed genes between control groups and LPS treated groups. (D) Cell viability of LPS-stimulated pericytes pretreated with inhibitors of different PCD. (E) The levels of lipid peroxidation, ferrous iron, GSH and GSH/GSSG ratio of LPS-stimulated pericytes pretreated with Fer-1. (F) FITC-BSA leakage in endothelial cells. (G) Flow cytometry analyses of ferroptosis of $CD31^{-}CD140b^{+}$ cells (pericytes) in the lung of mice. (n = 8/group) (H) Western blotting analysis of pericyte marker (PDGFR-β and NG2) in the lung tissues. (n = 3/group) (I) Laser confocal microscopy analysis of the pulmonary networks. (NG2, green, pericyte marker; CD31, red, endothelial cell marker. Bar = 50 μm). (n = 8/group) (J) Representative images of Evens-Blue leakage in the lung tissues. (n = 8/group) (K) Representative TEM images of tight junctions in pulmonary vessels. (Green arrow indicate the tight junction. Bar = 1 μm) (L) Wet weight to Dry weight ratio of lung in septic rats treated by Fer-1. (n = 8/group) (M) Inflammatory factors levels (IL-6 and TNF-α) in serum. (n = 8/group) (N) Survival curves of rats undergoing sham surgery, CLP and Fer-1 pretreatment. (n = 16/group)

Data were shown as mean ± SD. $^{**}p < 0.01$, $^{***}p < 0.001$. Statistical significance was determined by one-way ANOVA or two-sided Student's-test as appropriate. (For interpretation of the references to colour in this figure legend, the reader is referred to the Web version of this article.)

2.3. ACSL4 induces pericyte ferroptosis via mitochondrial dysfunction

The initiation and execution of ferroptosis are tightly regulated by the metabolism of iron, lipids, amino acids, and glutathione [18]. Metabolomics analysis in this study indicated significant metabolic reprogramming and disrupted lipid metabolism in pericytes following LPS treatment, leading to the generation of numerous ferroptosis substrates, including various phosphatidylethanolamines (PEs) and lyso-phosphatidylcholine (Lyso-PC) [18] (Fig. 3A). In contrast, no significant changes were observed in the other two main regulatory pathways of ferroptosis, namely iron metabolism and redox metabolism. ACSL4 is a key effector molecule in ferroptosis and a regulator of lipid metabolism. Its expression was significantly upregulated by 229.59 % in pericytes after LPS treatment (Fig. 3B–Supplementary data 5A). ACSL4

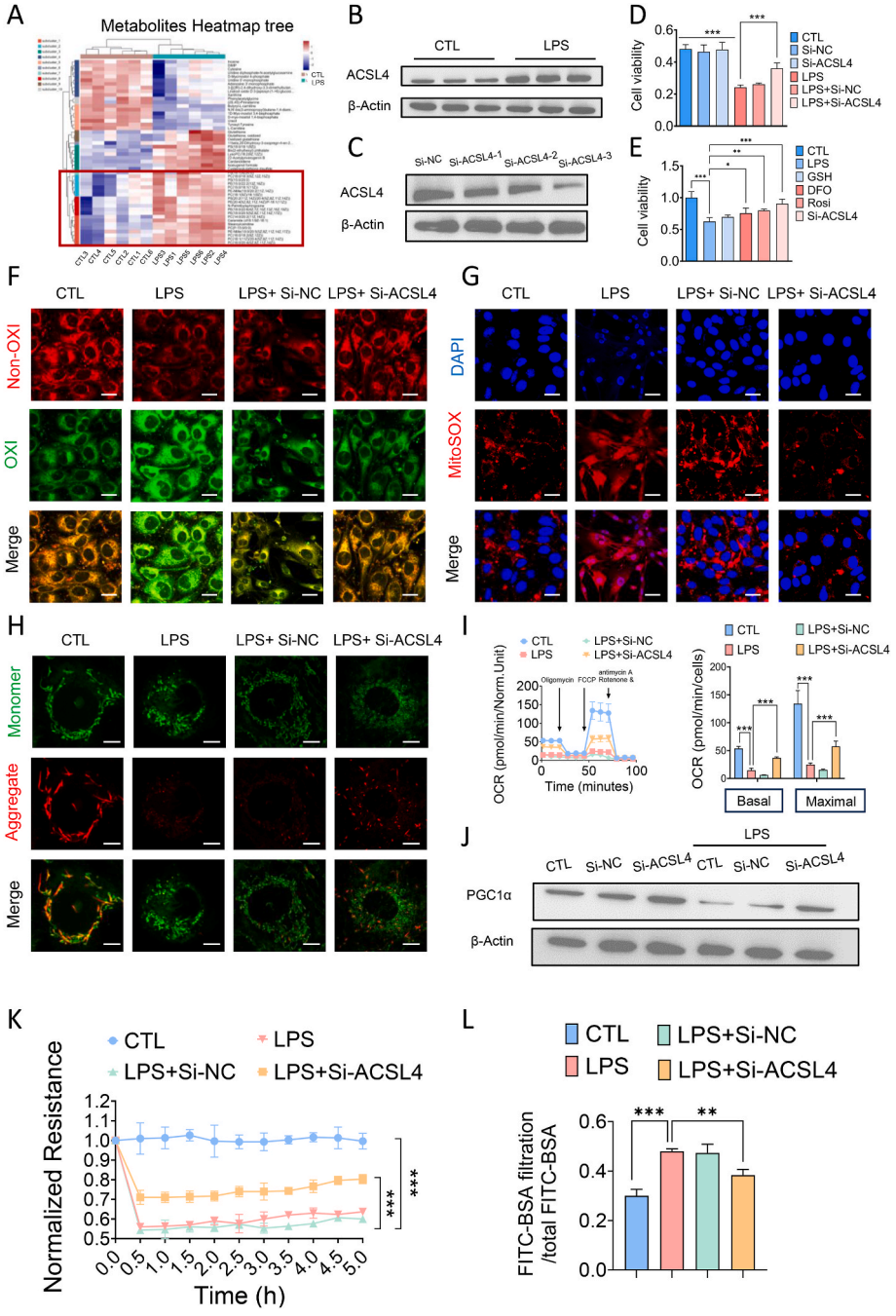

Fig. 3. ACSL4 induced pericytes ferroptosis via damaging mitochondria function. (A) Heatmap of differentially metabolites between control groups and LPS treated groups. (n = 6/group) (B) Western blotting analysis of ACSL4 of pericytes after LPS treatment. (C) The relative expression level of ACSL4 after treatment in Si-NC and Si-ACSL4 of pericytes. (D) Cell viability of LPS-stimulated pericytes pre-treated with Si-ACSL4. (E) Cell viability of LPS-stimulated pericytes pre-treated with GSH, Deferoxamine (DFO), Rosiglitazone (Rosi) and Si-ACSL4. (F–H) Confocal images to observe lipid peroxidation (Bar = 25 μm), MitoSOX (Bar = 25 μm) and mitochondria membrane potential (Bar = 10 μm) of LPS-stimulated pericytes after being transfected with Si-ACSL4. (I) Effects of Si-ACSL4 on the mitochondria respiration in pericytes. (J) The relative expression level of PGC-1α after treatment in Si-ACSL4 of pericytes. (K) Transendothelial electrical resistance (TER) of endothelial cells. (L) FITC-BSA leakage in endothelial cells.
For in vitro experiments or cell samples, n = 3 for each group. Data were shown as mean ± SD. **p < 0.01, ***p < 0.001. Statistical significance was determined by one-way ANOVA or two-sided Student's-test as appropriate.

knockdown in pericytes was achieved through transfection with ACSL4-shRNA adenovirus-3 (Fig. 3C–Supplementary data 5B). We observed that ACSL4 knockdown significantly improved pericyte viability (Fig. 3D). Further investigations using different ferroptosis inhibitors targeting iron metabolism, redox metabolism, and ACSL4 expression revealed that both an ACSL4 inhibitor, rosiglitazone, and ACSL4 knockdown significantly enhanced pericyte viability (Fig. 3E). Confocal imaging demonstrated a significant reduction in lipid peroxidation intensity following ACSL4 knockdown in pericytes, indicating an inhibitory effect on ferroptosis (Fig. 3F).

Mitochondrial fatty acid β-oxidation, a primary pathway for fatty acid catabolism, is closely associated with ferroptosis [30]. To further elucidate the mechanism of ACSL4-induced ferroptosis in pericytes during sepsis, we examined the impact of ACSL4 knockdown on key mitochondrial function indicators, including mitochondrial respiration, mitochondrial ROS production, and mitochondrial membrane potential in LPS-stimulated pericytes. Confocal imaging revealed that mitochondrial ROS production was significantly increased in pericytes following LPS stimulation (Fig. 3G), whereas ACSL4 knockdown markedly reduced mitochondrial ROS levels (Fig. 3G). Additionally, mitochondrial membrane potential was elevated in the ACSL4 knockdown group (Fig. 3H). Seahorse analyses indicated that ACSL4 knockdown significantly improved both basal mitochondrial respiration and maximal respiration capacity in LPS-stimulated pericytes (Fig. 3I). Furthermore, the transcriptional coactivator peroxisome proliferator-activated receptor gamma coactivator 1-alpha (PGC-1α), which plays a crucial role in regulating mitochondrial biogenesis, was significantly downregulated in pericytes post-LPS stimulation. ACSL4 knockdown significantly increased the expression of PGC-1α in pericytes (Fig. 3J–Supplementary data 5C). Finally, we assessed the impact of ACSL4 knockdown on the vascular endothelial cell (VEC) barrier and observed a significant decrease in TEER and BSA-FITC leakage, indicating improved endothelial leakage (Fig. 3K–L). These results suggest that ACSL4 induces ferroptosis in pericytes during sepsis, primarily through impairing mitochondrial function.

The enhanced β-oxidation associated with the upregulation of PGC1α expression may increase ROS production, leading to lipid peroxidation and cell death. To rule out this possibility, we examined a range of indicators of lipid peroxidation as well as redox balance in pericytes. Our results revealed that the content of LPO in pericytes following knocking down ACSL4 was comparable to that of negative control group with no significant difference, indicating that knockdown of ACSL4 alone did not cause lipid peroxidation in pericytes (Supplementary data 5D). We further examined the effect of knocking down ACSL4 on the expression level of GPX4 and COX2, as well as the content of GSH and ratio of GSH/GSSG. WB results showed that knocking down ACSL4 in pericytes had no significant effect on the expression level of GPX4 and significantly reduced the expression level of COX2 in pericytes (Supplementary data 5E). Knocking down ACSL4 in pericytes significantly reduced the expression of COX2 and increased the expression of GPX4 following LPS treatment. In addition, knocking down ACSL4 in pericytes significantly increased the content of GSH as well as ratio of GSH/GSSG in LPS-treated pericytes. These results showed that knocking down ACSL4 enhanced the antioxidant system in pericytes rather than inducing lipid peroxidation.

To further detect the effect of ACSL4 on ferroptosis of pericytes, we overexpressed ACSL4 in pericytes by lentiviral transfection (Supplementary data 5F) and examined the effects of the overexpression of ACSL4 in pericytes on cell viability, the contents of intracellular lipid ROS and LPO and the expression of PGC1α. The results showed that the overexpression of ACLS4 in pericytes significantly decreased the pericytes viability by 20.33 % compared with the CTL group (Supplementary data 5G). Overexpression of ACSL4 in combination with LPS treatment exacerbated the pericytes damage, with a significant decrease in pericytes viability of 40.01 % compared with the LPS-treated group alone (Supplementary data 5G). Then we examined the level of lipid peroxidation and found that the overexpression of ACSL4 alone did not cause significant lipid peroxidation in pericytes, and the combination of LPS treatment with overexpression of ACSL4 significantly exacerbated lipid peroxidation in pericytes compared with LPS treatment alone (Supplementary data 5H). The content of intracellular LPO and lipid ROS was increased by 30.49 % and 16.85 %, respectively. WB results showed that overexpression of ACSL4 significantly reduced the expression of PGC1α by 21.33 %, and overexpression of ACSL4 in combination with LPS treatment resulted in a 47 % decrease in the PGC1α expression level compared with LPS treatment alone (Supplementary data 5I).

2.4. Hippo/YAP signaling pathway regulates ACSL4-Mediated ferroptosis in pericytes

The Hippo pathway can sense various external stimuli and phosphorylate Yes-associated protein 1 (YAP1) through a kinase cascade, leading to its cytoplasmic retention and degradation [25,26]. The non-phosphorylated form of YAP1 can enter the nucleus, where it binds to transcription factors to activate target genes and exert transcriptional regulation [25,26]. Proteomic analysis in this study revealed that the Hippo pathway was significantly downregulated in pericytes following the LPS challenge (Fig. 4A). Immunofluorescence showed a significant increase in the nuclear translocation of YAP1 (Fig. 4B), and western blotting confirmed a substantial increase in YAP1 expression and a decrease in p-YAP1 after LPS treatment (Fig. 4C–Supplementary data 6A,6B).

To further investigate the role of YAP1 in ACSL4-induced ferroptosis of pericytes during sepsis, we knocked down YAP1 in pericytes using YAP1-shRNA adenovirus-3 (Fig. 4D–Supplementary data 6C). We observed that YAP1 knockdown reduced ACSL4 expression in pericytes under normal conditions and after LPS treatment (Fig. 4E–Supplementary data 6D). Furthermore, YAP1 knockdown significantly improved pericyte viability (Fig. 4F), and confocal imaging showed that YAP1 knockdown attenuated the accumulation of lipid peroxidation in pericytes (Supplementary data 6E). ELISA results indicated that YAP1 knockdown increased GSH and the GSH/GSSG ratio levels while decreasing lipid peroxidation and ferrous iron levels in pericytes (Fig. 4G). To further detect the effect of YAP1 on ferroptosis of pericytes, we overexpressed YAP1 in pericytes by lentiviral transfection (Supplementary data 6F). We examined the effects of overexpression of YAP1 on pericytes viability, the content of lipid ROS and LPO content and the expression of ACSL4 in pericytes. The results showed that the cell activity after overexpression of YAP1 in pericytes did not change significantly compared with the negative control group (Supplementary data 6G). However, overexpression of YAP1 in combination with LPS treatment exacerbated pericytes damage significantly and pericytes viability was significantly decreased by 31.21 %, compared with the LPS-treated group alone (Supplementary data 6H). Then we examined the level of lipid peroxidation, and found that overexpression of YAP1 alone did not cause significant lipid peroxidation in pericytes, and overexpression of YAP1 in combination with LPS treatment significantly exacerbated lipid peroxidation in pericytes, compared with LPS treatment alone (Supplementary data 6G). The content of intracellular LPO and lipid ROS was significantly increased by 27.11 % and 12.18 %, respectively (Supplementary data 6G). WB results showed that overexpression of YAP1 in pericytes significantly upregulated the expression of ACSL4 by 48.33 % without LPS treatment, and overexpression of YAP1 in combination with LPS treatment upregulated the expression of ACLS4 by 25.52 %, compared with LPS treatment alone (Supplementary data 6I).

These data suggest that the Hippo/YAP1 axis promotes ACSL4 expression in pericytes, and YAP1 knockdown attenuates ACSL4-mediated ferroptosis in pericytes during sepsis.

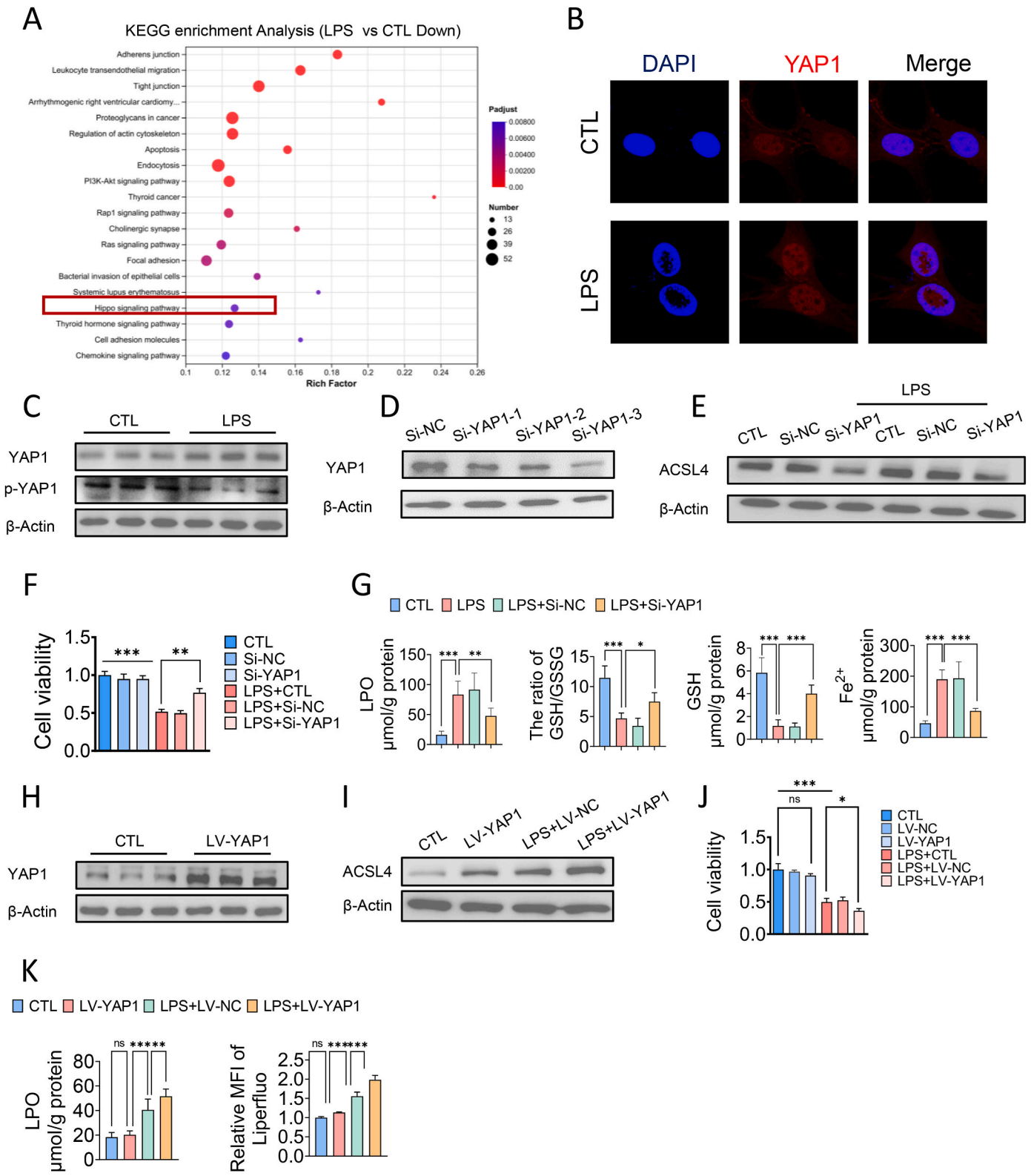

Fig. 4. Hippo/YAP signaling pathway regulated the expression of ACSL4 and ferroptosis in pericytes. (A) KEGG pathway (downregulated) of differentially expressed genes between control groups and LPS treated groups. (B) Immunofluorescence analysis of the nuclear translocation of YAP1. (C) Western blotting analysis of YAP1 of pericytes after LPS treatment. (D) The relative expression level of YAP1 after treatment in Si-NC and Si-YAP1 of pericytes. (E) The relative expression level of ACSL4 after treatment in Si-YAP1 of pericytes. (F) Cell viability of LPS-stimulated pericytes pre-treated with Si-YAP1. (G) The levels of lipid peroxidation, GSH/GSSG ratio, GSH and ferrous iron of LPS-stimulated pericytes pretreated with Si-YAP1.

For in vitro experiments or cell samples, n = 3 for each group. Data were shown as mean ± SD. *p < 0.05, *p < 0.01, ***p < 0.001. Statistical significance was determined by one-way ANOVA or two-sided Student's-test as appropriate.

2.5. Pericyte-specific ACSL4 knockout improved pulmonary vascular barrier function in sepsis

Upregulated ACSL4 expression in pericytes promotes ferroptosis and contributes to vascular barrier dysfunction following LPS stimulation. Given the significant association between pericyte ACSL4 levels and pericyte damage in sepsis, we utilized pericyte-specific ACSL4 knockout mice to evaluate the specific role of ACSL4 in pericyte ferroptosis and loss during sepsis. ACSL4 deletion in pericytes was achieved using the Cre-LoxP system, with genotyping confirmed by PCR (Table 1, Table 2 and Supplementary data 7). Compared with Flox mice, the colocalization of ACSL4 with pericytes (NG2) was significantly lower in the lung tissues of PDGFRβ-creERT2 ACSL4flox/flox mice (Fig. 5A).

We first assessed pulmonary vascular leakage and found that the extravasation of Evans blue in the lung tissues of PDGFRβ-creERT2 ACSL4$^{flox/flox}$ mice was significantly reduced compared to Flox mice (Fig. 5B). We further examined the effect of pericyte-specific ACSL4 knockout on pericyte ferroptosis and loss. The level of lipid ROS in the lung tissues of PDGFRβ-creERT2 ACSL4$^{flox/flox}$ mice was decreased in sepsis compared to Flox sepsis mice (Fig. 5C). Immunostaining showed a significant increase in the expression of NG2 (Fig. 5D), and western blotting revealed a significant upregulation of NG2 and PDGFR-β in PDGFRβ-creERT2 ACSL4$^{flox/flox}$ mice compared to Flox mice (Fig. 5E), indicating that pericyte loss was significantly attenuated by pericyte-specific ACSL4 knockout. Additionally, the wet/dry ratio of the lungs was reduced due to pericyte-specific ACSL4 knockout (Fig. 5F).

Regarding animal survival (Fig. 5G), only three Flox mice survived beyond 24 h, with a mean survival time of 17.35. In contrast, six PDGFRβ-creERT2 ACSL4flox/flox mice survived for more than 72 h, with a significantly higher mean survival time of 60.6 h. The 72-h survival rate was 12.5 % (2/16) for Flox mice and 37.5 % (6/16) for PDGFRβ-creERT2 ACSL4flox/flox mice, respectively.

These findings highlight that pericyte-specific ACSL4 knockout significantly improves pulmonary vascular barrier function and survival in sepsis, primarily by attenuating pericyte ferroptosis and loss.

Table 1

PCR Reaction & Cycling				
Acsl4-Flox				
Primer	Sequence (5'→3')			Primer Type
P1	AGTTAGCAGAGGGAGGCTGA			Forward
P2	GGCTTGCTTGTGGCACATTA			Reverse
PCR Reaction System	Reaction Component			Volume (μl)
	ddH2O			7.0
	2 × transTaq-T PCR SuperMix			10.0
	P1 (10 pmol/μl)			0.5
	P2 (10 pmol/μl)			0.5
	Genomic DNA (50–100 ng/μl)			2
	Total			20
	2 × transTaq-T PCR SuperMix from TransGen Biotech (Code number:AS122)			
Cycling Reaction	Step	Temp	Time	Note
	1	94 °C	3 min	
	2	94 °C	30 s	
	3	60 °C	30 s	
	4	72 °C	30 s	34 repeats to 2
	5	72 °C	5 min	
	6	12 °C	Hold	
Genotype	Wild type : one band with 318 bp			
	Heterozygote : two bands with 318 and 372 bp			
	Homozygote : one band with 372 bp			
Pdgftb-creERT2				
Primer	Sequence (5'→3')			Primer Type
P3	GAACTGTCACCGGGAGGA			Transgene Forward
P4	AGGCAAATTTTGGTGTACGG			Transgene Reverse
P5	CAAATGTTGCTTGTCTGGTG			Internal Positive Control Forward
P6	GTCAGTCGAGTGCACAGTTT			Internal Positive Control Reverse
PCR Reaction System	Reaction Component			Volume (μl)
	ddH2O			6.0
	2 × transTaq-T PCR SuperMix			10.0
	P3 (10 pmol/μl)			0.5
	P4 (10 pmol/μl)			0.5
	P5 (10 pmol/μl)			0.5
	P6 (10 pmol/μl)			0.5
	Genomic DNA (50–100 ng/μl)			2
	Total			20
	2 × transTaq-T PCR SuperMix from TransGen Biotech (Code number:AS122)			
Cycling Reaction	Step	Temp	Time	Note
	1	94 °C	3 min	
	2	94 °C	30 s	
	3	60 °C	30 s	
	4	72 °C	30 s	34 repeats to 2
	5	72 °C	5 min	
	6	12 °C	Hold	
Genotype	Tg : ~400 bp			
	Control : 200 bp			

Table 2

mice ID and message			
mice ID	Sex	genotype	
		Acsl4-Flox	Pdgftb-creERT2
B1	♂	HO	+
B2	♂	HO	+
B3	♂	HO	–
B4	♂	HO	+
B5	♂	HO	–
B6	♂	HO	–
B7	♀	HO	+
B8	♀	HO	–
B9	♀	HO	+
B10	♀	HO	+
B11	♀	HO	–
B12	♀	HO	+
B18	♀	HO	+
B19	♀	HO	–
B21	♀	HO	+
B22	♂	HO	–
B24	♂	HO	–
B26	♂	HO	–
B34	♂	HO	–
B35	♂	HO	+
B38	♀	HO	+
B39	♀	HO	–
B40	♀	HO	–
B43	♂	HO	–
B44	♂	HO	+
B50	♀	HO	–
B51	♀	HO	–
B52	♀	HO	–
B55	♂	HO	–
B56	♂	HO	–

Note: HO:Homozygote.+: Positive, -: Negative.

2.6. Si-ACSL4@LNP-AA/NG2 attenuated pericyte loss and improved multiple organ function in sepsis

Nanoparticle-based drug delivery systems (DDS) are promising in sepsis treatment research· In this study, we developed pericyte-targeting liposomes encapsulating ACSL4 shRNA adenovirus. The ability to specifically knock down ACSL4 expression in pericytes while minimizing systemic toxicity is a major advantage of nano-DDS over other agents. We selected two peptides, TAASGVRSMH and CPRECES, modified on the liposome surface to target pericyte markers NG2 and Aminopeptidase A, respectively [31–33]. The structure and purity of these peptides were validated using Mass Spectrometry (MS), High-Performance Liquid Chromatography (HPLC), and Nuclear Magnetic Resonance

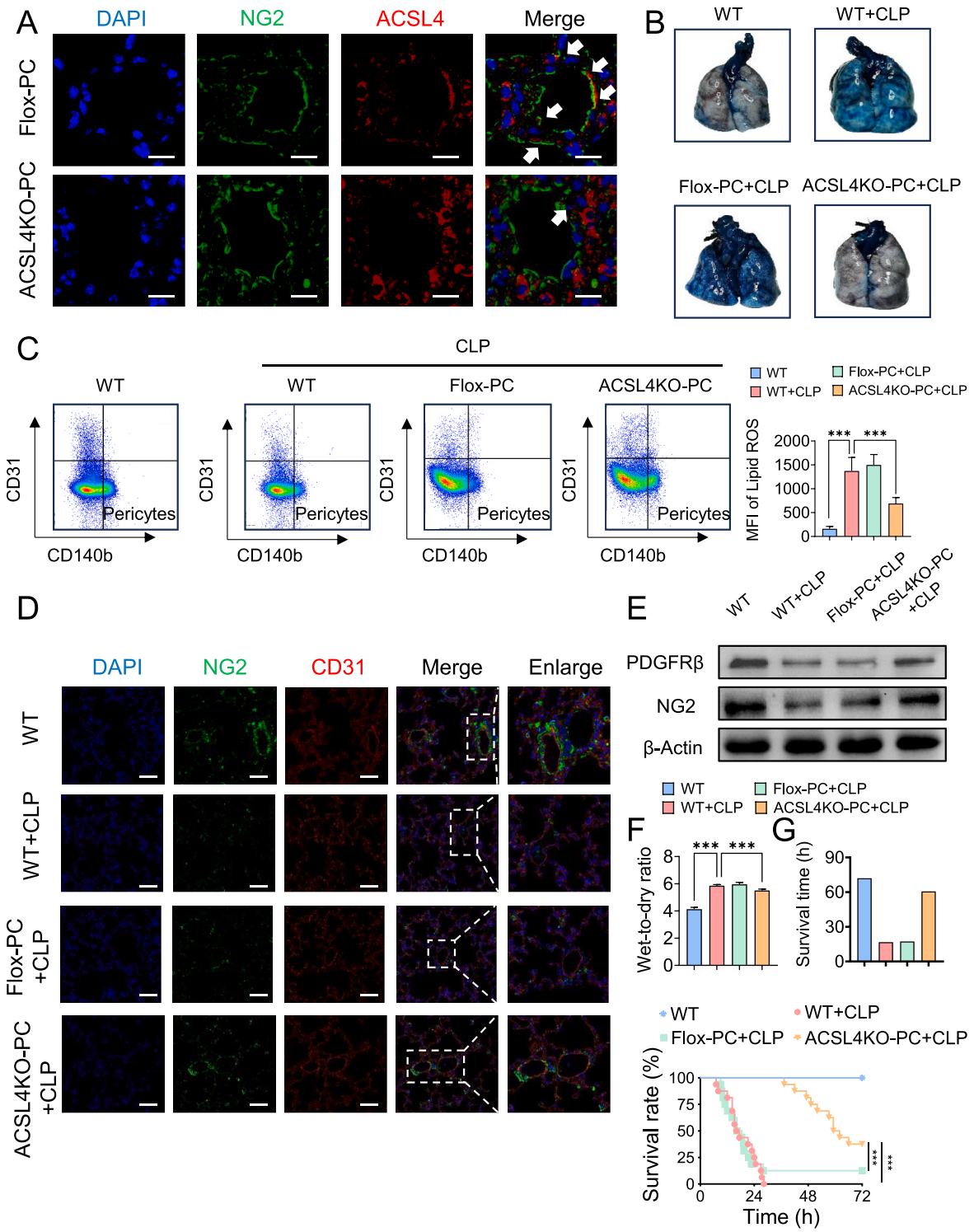

Fig. 5. Pericytes-specific ACSL4 knockout improved pulmonary vascular barrier function in sepsis. (A) Representative images of immunofluorescence co-localization of ACSL4 and NG2 in the mouse lung tissues. (n = 8/group) (B) Representative images of Evens-Blue leakage in the lung tissues. (n = 6/group) (C) Flow cytometry analyses of ferroptosis of $CD31^{-}CD140b^{+}$ cells (pericytes) in the lung of mice. (n = 8/group) (D) Laser confocal microscopy analysis of the pulmonary networks. (NG2, green, pericyte marker; CD31, red, endothelial cell marker. Bar = 50 μm). (n = 8/group) (E) Western blotting analysis of pericyte marker (PDGFR-β and NG2) in the lung tissues. (n = 3/group) (G) Survival curves of rats undergoing sham and CLP surgery. (n = 16/group)
Data were shown as mean ± SD. ***$p < 0.001$. Statistical significance was determined by one-way ANOVA as appropriate. (For interpretation of the references to colour in this figure legend, the reader is referred to the Web version of this article.)

spectroscopy (NMRS) (Supplementary data 8A-8B). Si-ACSL4@LNP-AA/NG2 appeared uniform spheres with ideal dispersion under a transmission electron microscope (Supplementary data 8C). The hydrodynamic particle size of Si-ACSL4@LNP-AA/NG2 was measured at 101.8 ± 6.23 nm (Supplementary data 8D), with a PDI of 0.1775 ± 0.005 (Supplementary data 8E). The zeta potential was −10.49 ± 1.285 mV (Supplementary data 8F). These characteristics were not significantly different between Si-ACSL4@LNP-AA/NG2 and Si-NC@LNP-AA/NG2.

In vivo, the biosecurity of Si-ACSL4@LNP-AA/NG2 was verified by H&E staining of major organs (heart, kidney, liver, lung) and blood biochemical index determination. H&E staining showed no significant inflammation or necrosis (Supplementary data 8G). Liver, kidney, and cardiac function indexes, including aspartate aminotransferase (AST), phenylalanine aminotransferase (ALT), serum creatinine (Crea), and blood urea nitrogen (Urea), were close to normal levels and did not significantly differ between the Si-ACSL4@LNP-AA/NG2 group and the Si-NC@LNP-AA/NG2 group (Supplementary data 8H). These results demonstrated low biotoxicity of Si-ACSL4@LNP-AA/NG2. Immunofluorescence and flow cytometry confirmed the targeted binding of Si-ACSL4@LNP-AA/NG2 to pericytes in vivo and in vitro, showing substantial co-localization in lung tissues (Supplementary data 8I). The binding rate of pericytes with Si-ACSL4@LNP-AA/NG2 was 58.00 % ± 3.364 %, significantly higher than that of Si-ACSL4@LNP (22.67 ± 2.517 %) and PBS (21.67 % ± 3.786 %) (Supplementary data 8J). These results indicate effective targeting of pericytes by Si-ACSL4@LNP-AA/NG2.

To assess the effect of pericyte-targeting liposomes (Si-ACSL4@LNP-AA/NG2) on sepsis-induced pericyte ferroptosis and pulmonary vascular barrier dysfunction, we administered Si-ACSL4@LNP-AA/NG2 to animals before CLP via tail vein injection. Flow cytometry revealed a 63.99 % reduction in lipid ROS levels in lung pericytes following Si-ACSL4@LNP-AA/NG2 treatment (Fig. 6A). Si-ACSL4@LNP-AA/NG2 significantly attenuated pericyte loss, as evidenced by upregulated expression of NG2 and PDGFR-β in western blotting (Fig. 6C–Supplementary data 9B) and immunostaining (Fig. 6B–Supplementary data 9C). Further analysis showed that Si-ACSL4@LNP-AA/NG2 treatment reduced pulmonary vascular leakage, as indicated by decreased extravasation of FITC-BSA (Fig. 6E–Supplementary data 9A) and Evans blue (Fig. 6D). Lung function significantly improved with treatment, demonstrated by a decreased wet/dry ratio, improved blood gas indices, and better pathological lung structure (Supplementary data 9D-9G). Since vascular dysfunction is a core feature and trigger of multiple organ dysfunction, we assessed the impact of Si-ACSL4@LNP-AA/NG2 on blood flow and organ function. Treatment significantly improved blood flow to the intestines, liver, and kidneys (Supplementary data 9H) and reduced organ injury markers (Supplementary data 9I), including ALT, AST, Crea, Urea, and cTnT. Additionally, Si-ACSL4@LNP-AA/NG2 significantly lowered serum levels of IL-6 and TNF-α by 38.22 % and 57.07 %, respectively (Fig. 6F), and improved animal survival (Fig. 6G) (see Fig. 7).

These findings suggest that Si-ACSL4@LNP-AA/NG2 effectively protects against pericyte impairment in sepsis, thereby alleviating vascular barrier dysfunction and improving sepsis prognosis.

3. Discussion

Sepsis is defined as life-threatening organ dysfunction caused by a dysregulated host systemic inflammatory and immune response to infection [34]. Over the decades, an advanced understanding of host-microorganism interactions has gradually unmasked the genuine nature of sepsis, leading to new definitions and novel therapeutic approaches [35–37]. Acute lung injury following sepsis results in increased vascular permeability, causing noncardiogenic pulmonary edema, which impairs oxygenation and ventilation and plays a key role in the pathological process of multiple organ dysfunction [38,39].Recently, the central role of pericyte loss in sepsis and its regulation of vascular barrier integrity has been recognized as a promising target for therapeutic interventions [7,8]. However, the precise mechanism of pericyte loss in sepsis remains unclear and limited effective treatments for pericytes damage haves been developed. Thus, deepening our understanding of pericytes loss pathophysiological intricacies and discovering molecular mechanisms would be essential for the exploration of targeted therapeutic agents. Our study combined single-cell sequencing in vivo with proteomics and metabolomics in vitro to investigate the mechanism of pericyte impairment following sepsis.

Ferroptosis is an iron-dependent, non-apoptotic programmed cell death mode distinguished by a disruption of iron metabolism and iron-dependent accumulation of lipid peroxides, which was first introduced by Dixon et al., in 2012 [18]. Ferrous iron interacts with polyunsaturated fatty acids (PUFAs) in cell membrane through Fenton reaction, which produce lipid hydroperoxides (LOOHs), this process named as lipid peroxidation [18]. Excessive LOOHs accumulates and the antioxidant system breaks down triggering cellular ferroptosis. Recent studies have demonstrated that in settings such as infection, inflammation and cancer, disruption of this homeostasis can promote ferroptosis and result or exaggerate diseases [19]. For instance, immune cells such as macrophages and T cells themselves undergo ferroptosis, which causes a reduction in numbers and function of immune cells. In turn, cells undergoing ferroptosis can be recognized by immune cells and trigger inflammatory responses. Therefore, ferroptosis is closely associated with infection and inflammatory responses. Changhong Miao et al. have showed neutrophil extracellular traps (NETs)-induced METTL3 modification and the ferroptosis were related to the pathogenesis of sepsis-associated acute lung injury [40]. Jianan Ren et al. have discovered that STING promotes sepsis-induced multiple organ injury by inducing macrophage ferroptosis in a cGAS- and interferon-independent manner [41]. Collectively, these insights provide meaningful guidance for the exploration of the relationship between sepsis and ferroptosis.

Pericytes loss has been views as the development and progression of various diseases, such as diabetes, Alzheimer's diseases, sepsis, stroke and traumatic brain injury [7,8]. In diabetic retinopathy (DR), a major complication of diabetes, pericytes death via apoptosis is involved and is verified by both patients and animal models of DR [42]. In addition, pericytes loss in DR is may be induced by the migration of retinal pericytes, which is regulated by autophagy [43]. Podocytes, which are pericyte-like cells, play a crucial role in the progression of diabetic nephropathy (DN) [44]. Jiang et al. have pointed out that autophagy, mitotic catastrophe, anoikis, necrosis and pytoptosis are implicated in podocytes loss in DN [45]. In aging and neurodegenerative diseases, apoptosis is believed to induce pericytes loss, as pericytes apoptosis has been proved in the retina and hippocampus of Alzheimer's diseases patients [46]. As for sepsis, the relationship between pericytes dysfunction and sepsis-induced microvascular dysfunction is highlighted and pericytes loss serves as a hallmark of severe shock and severe sepsis [47,48]. Chen et al. have demonstrated that pericytes loss has been observed in the lung and heart tissues following sepsis [14], which was accompanied by severe impairment of microvascular dysfunction. However, this phenomenon is not related to apoptosis of pericytes. The mechanism underlying pericytes loss in the lung tissues following sepsis remains unknown. Our previous study has proved that pericytes transplantation and pericytes-derived microvesicles can improve vascular function and animal survival [11]. Therefore, the exploration of the precise mechanism of pericytes loss and therapeutic strategies targeting pericytes in sepsis is important and needed.

To explore the mechanism of pericytes loss in sepsis, we combined single-cell sequencing with proteomics and found that ferroptosis is implicated in pericyte damage in sepsis. Ferroptosis has been proved to play an important role in acute lung injury in LPS-induced sepsis, using GPX4 and SLC7A11 as monitoring markers [49]. Ferrostatin-1 (Fer-1)

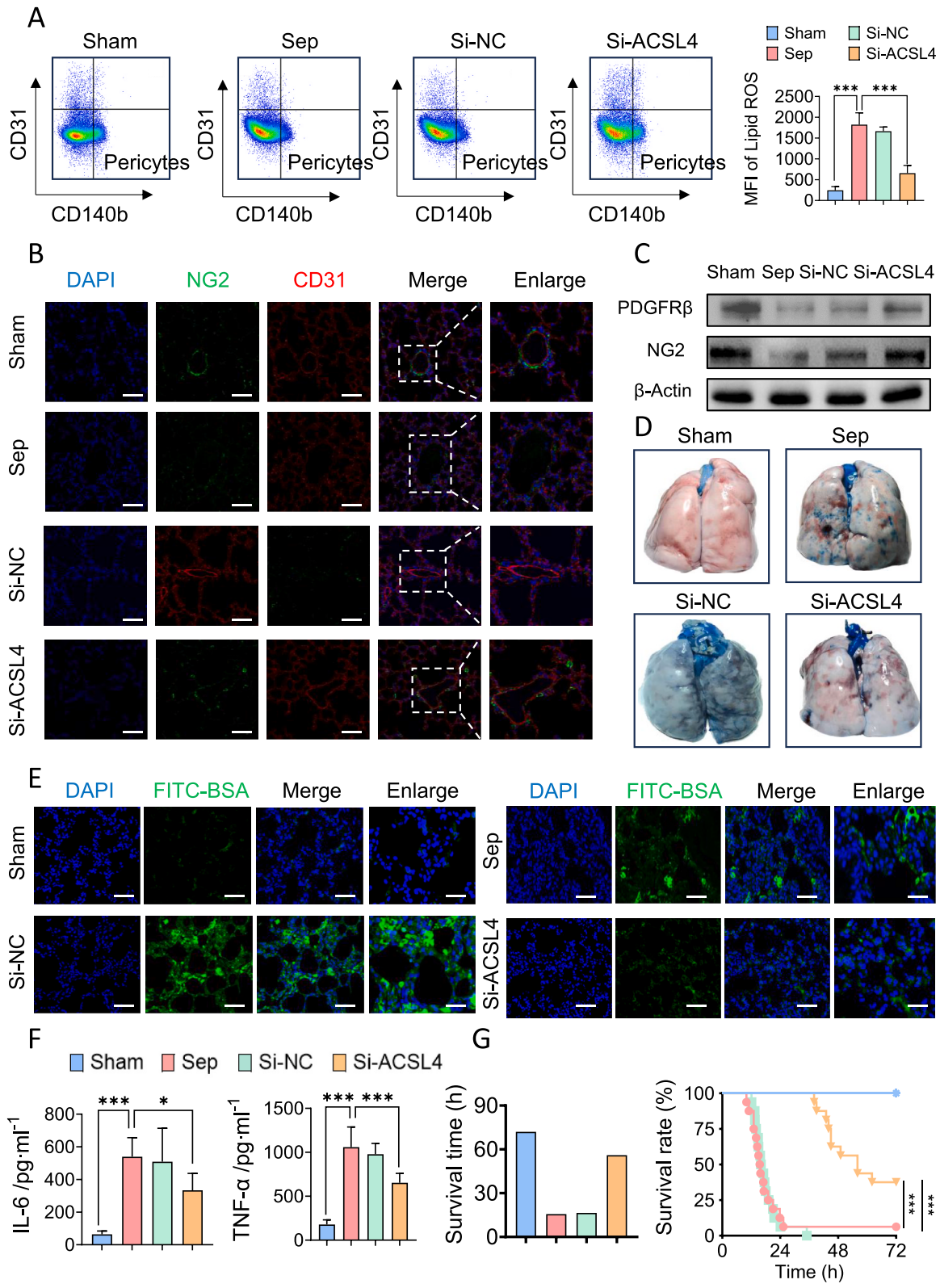

Fig. 6. Pericytes targeting liposomes encapsulating ACSL4 shRNA adenovirus inhibited pericytes ferroptosis and improved pulmonary vascular barrier function. (A) Flow cytometry analyses of ferroptosis of $CD31^{-}CD140b^{+}$ cells (pericytes) in the lung of mice. (n = 8/group) (B) Laser confocal microscopy analysis of the pulmonary networks. (NG2, green, pericyte marker; CD31, red, endothelial cell marker. Bar = 50 μm). (n = 8/group) (C) Representative images of Evens-Blue leakage in the lung tissues. (n = 6/group) (D) Western blotting analysis of pericyte marker (PDGFR-β and NG2) in the lung tissues. (n = 3/group) (E) Representative images of FITC-BSA leakage in the lung tissues. (Blue, DAPI; green, FITC-BSA. Bar = 50 μm) (F) Inflammatory factors levels (IL-6 and TNF-α) in serum. (n = 8/group) (G) Survival curves of rats undergoing sham surgery, CLP and Fer-1 liposomes pretreatment. (n = 16/group)

Data were shown as mean ± SD. *$p < 0.05$, ***$p < 0.001$. Statistical significance was determined by one-way ANOVA as appropriate. (For interpretation of the references to colour in this figure legend, the reader is referred to the Web version of this article.)

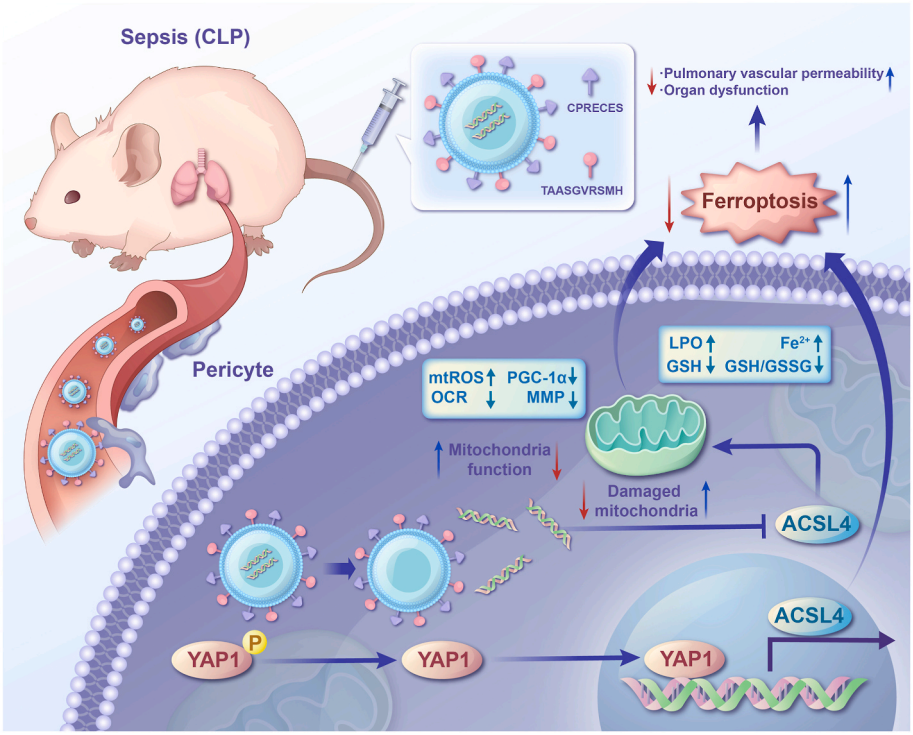

Fig. 7.

can improve lung histological structure and have great benefits [49]. Other ferroptosis inhibitors also exert therapeutic effects. Electroacupuncture (EA) inhibits LPS-induced ferroptosis in alveolar epithelial cells by activating a7nAchR and attenuated the lung inflammatory response [50]. Itraconate inhibits macrophage ferroptosis via the Nrf2 pathway [51]. Therefore, we further investigate the relationship between pulmonary vascular pericytes loss and ferroptosis. Among the various inhibitors tested, including those targeting apoptosis, autophagy, necroptosis, ferroptosis, and pyroptosis, we found that Fer-1 significantly rescued pericyte viability and attenuated ferroptosis. Fer-1 alleviated ferroptosis, reduced pericyte loss, and improved pulmonary vascular barrier function and survival in septic rats. These results suggest that ferroptosis is a primary mechanism of pericyte damage and death in sepsis, making it a potential therapeutic target.

Metabolomics revealed significant metabolic reprogramming and lipid metabolism disorder in pericytes following LPS treatment. Lipid metabolism is crucial for the onset and execution of ferroptosis. At the first, polyunsaturated fatty acids (PUFAs) such as arachidonic acid (AA) are synthesized into lipids and inserted into membrane phospholipids to form PUFA-PL complexes, which is catalyzed by Acyl-CoA synthetase long-chain family member 4 (ACSL4) [18]. Then, peroxidases (LOXs) can oxidize PUFA-PL complexes and ferroptosis is activated. The lipid metabolism includes synthesis, storage and catabolism of lipid, which all affect the concentration of ferroptosis substrate and further determine the susceptibility of cells to ferroptosis. Zhuang L et al. have showed that energy stress-induced activated AMPK inhibits ferroptosis via reducing the biosynthesis of PUFAs [18]. ACSL4, a key regulator of lipid metabolism and a known ferroptosis executor was upregulated in pericytes after LPS stimulation [52–54]. Knockdown of ACSL4 inhibited ferroptosis and alleviated endothelial leakage. Using PDGFRβ-creERT2 mice to knockout ACSL4 in pericytes, we observed significant alleviation of ferroptosis, reduced pericyte loss, and improved pulmonary vascular barrier function in septic mice. Additionally, we developed pericyte-targeting liposomes encapsulating ACSL4-shRNA, which effectively protected against ferroptosis and pericyte loss and improved pulmonary vascular barrier function. Collectively, these findings highlight ACSL4 as a promising target for preventing and treating pericyte loss and vascular barrier dysfunction in sepsis.

The Hippo pathway is an evolutionarily conserved pathway that relays cell confluence signals to downstream gene expression, which controls tissue growth, organ size and development by regulating cell proliferation and self-renewal [24,25]. The Hippo pathway is composed of core kinases: mammalian Ste20-like kinases 1/2 (MST1/2), a large tumor suppressor 1/2 (LATS1/2) and the two major downstream effectors which are paralogous transcription coactivators: YAP and TAZ [24,25]. Recent studies have showed that Hippo pathway is closely related to ferroptosis [24,25]. The expressions of ACSL4, intracellular iron availability (TFRC: transferrin receptor) and ROS production (NOX2/NOX4) are all regulated by YAP [24]. Our study also revealed that pericytes' Hippo/YAP signaling pathway is significantly downregulated following LPS treatment. Yes-associated protein 1 (YAP1) and transcriptional coactivator TAZ are essential downstream effectors of the Hippo pathway, regulating cell proliferation. YAP1 can be phosphorylated and inactivated, leading to its retention in the cytoplasm. However, in the nucleus, YAP1 actively regulates transcription. We found that both the expression and nuclear translocation levels of YAP1 were significantly increased in pericytes after the LPS challenge. Knockdown of YAP1 downregulated ACSL4 expression and reduced ferroptosis in pericytes, indicating that YAP1 promotes ACSL4-mediated ferroptosis in sepsis.

Increasing evidence indicates that mitochondria are a primary source of intracellular ROS, with approximately 90 % of ROS produced in mitochondria [55]. The burst of mitochondrial ROS in sepsis causes significant oxidative damage to mitochondrial bioenergetics, leading to ferroptosis by inducing membrane peroxidation [56,57]. We found that knockdown of ACSL4 in pericytes increased the expression of peroxisome proliferator-activated receptor gamma coactivator 1-alpha (PGC-1α), reduced mitochondrial ROS generation, restored mitochondrial membrane potential, improved mitochondrial respiration, and alleviated ferroptosis, indicating a negative regulation of ACSL4 on PGC-1α, which induces pericyte ferroptosis. The potential oxidative damage associated with increased mitochondrial respiration and

β-oxidation brought by ACSL4 knockdown. However, contrary to expectations, the knockdown of ACSL4 in vivo and in vitro pericytes demonstrated a protective effect without a burst of cellular ROS accumulation. We observed the effect of ACSL4 knockdown on redox balance in pericytes and found that the knockdown of ACSL4 pericytes. Our results revealed that the content of LPO in pericytes following knocking down ACSL4 was comparable to that of negative control group with no significant difference, indicating that knockdown of ACSL4 alone did not cause lipid peroxidation in pericytes. In addition, knocking down ACSL4 in pericytes significantly increased the expression of GPX4 and the content of GSH as well as ratio of GSH/GSSG in LPS-treated pericytes. GPX4 is an important intracellular antioxidant enzyme responsible for removing lipid peroxides with high biological activity. If knocking down ACSL4 in pericytes reduces the production of these peroxides, pericytes may have enhanced the expression of GPX4 through a feedback mechanism to help restore the antioxidant status against oxidative stress. These changes may be a cellular response to adapt to a new lipid metabolic balance as well as to avoid excessive cellular stress.

Although our study discovered the potential mechanism of pulmonary vascular pericytes damage in sepsis, which are possibly related to its enhancement of ferroptosis, several limitations remain. Firstly, this study employed rodents as subjects, the impact of ferroptosis on post-sepsis pericytes loss and organ function in large animal models remains to be elucidated and will be the subject of future research. Secondly, while our focus was primarily on the post-sepsis pulmonary vascular pericytes damage effects and associated ferroptosis, the effect of ferroptosis on pericytes in other tissues and organs post-sepsis require in-depth investigation. When considering the clinical translation of pericyte-targeting liposomes, its several bottlenecks should be taken into accounts. Assessing the biocompatibility, toxicity, and long-term effects of nanomaterials is a crucial and complex task that often requires extensive animal studies and clinical trials. In addition, the synthesis processes of nanomaterials are often difficult to control, leading to significant differences in the physical and chemical properties between different batches. This lack of consistency poses challenges to predicting efficacy and safety in clinical applications. In the context of septicemic pulmonary vascular barrier dysfunction, therapeutic targeting pericytes strategies offers a promising direction. However, further studies are needed to comprehensively assess pericyte-targeting liposomes's protective or potentially adverse impacts on other tissues and organs in the post-sepsis context.

In conclusion, this study demonstrates that the YAP1/ACSL4/PGC1α axis promotes ferroptosis and pericyte loss in sepsis. Our findings underscore the therapeutic potential of targeting ACSL4 to treat pericyte loss and provide evidence that pericyte-targeting liposomes could treat pulmonary vascular leakage in sepsis. These findings offer a preclinical basis for interventions targeting pericyte loss in sepsis management.

CRediT authorship contribution statement

Yiyan Liu: Writing – original draft, Validation, Project administration, Methodology, Formal analysis, Data curation, Conceptualization. **Daiqin Bao:** Project administration, Methodology, Formal analysis, Data curation. **Han She:** Writing – review & editing, Investigation, Data curation, Methodology. **Zisen Zhang:** Formal analysis, Data curation, Conceptualization. **Shifeng Shao:** Methodology, Investigation, Formal analysis. **Zhengbin Wu:** Software, Project administration. **Yue Wu:** Software. **Qinghui Li:** Software. **Li Wang:** Writing – review & editing, Writing – original draft, Software, Formal analysis, Data curation. **Tao Li:** Writing – review & editing, Visualization, Supervision, Investigation. **Liangming Liu:** Writing – review & editing, Visualization, Supervision, Investigation, Funding acquisition, Data curation, Conceptualization.

Funding

This program is supported by Key Program of the National Natural Science Foundation of China. (Grant ID: 82330079)

Declaration of competing interest

There are no conflicts in this work to declare within the author reports.

Appendix A. Supplementary data

Supplementary data to this article can be found online at https://doi.org/10.1016/j.redox.2024.103353.

Materials and methods

1.Ethical approval

In the present study, all experiments followed the Guide for Care and Use of Laboratory Animals by America (National Institute of Health) and approved by Army.

Medical University's Ethics Committee and Research Council and Animal Care and Use Committee (Number. DHEC-2012-069).

2.Patients samples

Peripheral blood from 20 sepsis patients and 20 healthy volunteers was obtained from the Daping Hospital of Army Medical University. Pericytes were isolated using a flow cytometry sorting (MoFlo Astrios EQ, Beckman) system. Collection of samples was performed with the approval of the Ethics Committee at the Third Affiliated Hospital of Army Medical University (Trial registration: ClinicalTrials.gov, NCT01713205.). Sepsis was confirmed according to the Third International Consensus Definitions for sepsis and septic shock (Sepsis-3). Written informed consent was obtained from the patients or their next of kin before enrollment, including the collection of relevant clinical data. Patient confidentiality was preserved in accordance with the guidelines of the Declaration of Helsinki. The exclusion criteria were as follows: (1) under the age of 18 and (2) preexisting respiratory, cardiovascular, hepatic, renal, immunological, or hematological disease.

3.Animals' preparation and sepsis model

C57BL/6, PDGFRβ-creERT2 and ACSL4flox/flox mice were purchased from the Shanghai model Organisms Center. ACSL4 conditional knockout in pericytes mice (PDGFRβ-creERT2 ACSL4flox/flox) was generated from PDGFRβ-creERT2 and ACSL4flox/flox mice. Male and female Sprague–Dawley (SD) rats (8–12 weeks of age) were purchased from the Animal Research Center of the Daping Hospital (Army Medical Center). Animals were maintained in the animal facility of Daping Hospital, Army Medical University. Before experiments, all mice were acclimatized for 1 week. Animals of both sexes were used in the study. Age- and sex-matched (8–12 weeks) controls were used in each experiment.

Sepsis model was performed by cecal ligation and puncture (CLP) procedure as described. In brief, laparotomy was performed under anesthesia with pentobarbital sodium solution (45 mg/kg intraperitoneal), the cecum was gently exposed, the feces were concentrated at the end of the cecum, and then the cecum was punctured from the distal end of the cecum with a triangular needle for rats and double punctures (20-gauge needle) for mice to facilitate the free passage of feces into the peritoneal cavity. Afterward, the abdomen was closed by interrupted suture. Upon completion of the surgery, and they were subsequently fed with water until use. Rats were resuscitated using an intraperitoneal injection of 5 mL lactated ringer's solution and mice were resuscitated using an intraperitoneal injection of 1 mL lactated ringer's solution. 12 h after CLP, the peripheral blood and liver, kidney, heart and lung tissues were collected for subsequent experiments. Animal subjects with mean

arterial pressure at<70 mmHg or>30 % reduction at 12h following CLP were used for subsequent experiments. The success rate of the sepsis model was 82 % in this study.

4.Cell culture and reagents

Pericytes were isolated and cultured as previously described [12]. Morphological characterization and immunofluorescence characterization were observed via phase contrast microscopy and confocal laser scanning microscopy, respectively. (CLSM; SP5II, Leica Microsystems, Wetzlar, Germany). The cells were verified with cell surface markers, PDGFR-β (ab32570, Abcam), nerve/glial antigen 2 (NG-2; ab5320, Abcam), CD146 (ab75769, Abcam), α-smooth muscle actin (α-SMA; ab7817, Abcam), and platelet endothelial cell adhesion molecule (CD31; ab24590, Abcam). Pericytes were cultured in specific medium supplemented with 2 % fetal bovine serum and specific growth supplement. Pericytes were maintained at 37 °C in a humidified environment of 5 % CO2 and 95 % air.

LPS (O55:B5) was purchased from Sigma (America). Apoptosis inhibitor (NSC 15364; HY-108937), autophagy inhibitor (Chloroquine phosphate; HY-17589), necroptosis inhibitor (Necrostatin-7; HY-117200), ferroptosis inhibitor (Ferrostatin-1; HY-100579) and ACSL4 inhibitor (Rosiglitazone; HY-17386) were all purchased from MedChemExpress (America). Cell Counting Kit-8 was purchased from MedChemExpress (HY–K0301). A 24-well XFe plate (102340–100), cell mitochondrial substrate stress test kit, Seahorse XF Dulbecco's Modified Eagle Medium (DMEM), Seahorse XF 100 mM pyruvate solution, and Seahorse XF 200 mM glutamine solution were purchased from Agilent Cell Analysis Technology (America). MitoSox Red (M36006) was procured from Invitrogen (America). Pericytes specific medium, pericytes growth supplement and antibiotics were procured from ScienCell (America). The JC-1 fluorescent probe was purchased from Beyotime (C2005; China). LPO Elisa Kit (A106-1-2) was purchased from NanJing JianCheng Bioengineering Institute (China). Iron Assay Kit (I291) and Lipid Peroxidation Probe -BDP 581/591 C11 (L267) were purchased from Dojindo (Japan).

5.Vascular permeability of the lungs

FITC-BSA (9 mg/kg) was injected via the jugular vein in rats. 2 h after the administration, the abdominal cavity was opened, and the abdominal aorta was cut open, slowly infusing the normal saline solution through the jugular vein until the lung tissue became white. The lower lobe of the right lung was embedded with OCT glue, and a frozen section (section thickness 10–15 μm) was performed. Samples were fixed with 4 % paraformaldehyde for 30 min, permeated with 0.1 % Triton-X for 3 min, and incubated with DAPI (1:50) at 37 °C for 30 min. The FITC-BSA exudation in lung tissue was observed under a laser confocal microscope and the average fluorescence intensity of FITC in lung tissue was used to represent the pulmonary vascular barrier.

Evens Blue (60 mg/kg) was injected via jugular catheter in rats. 30 min after the administration, the abdominal cavity was opened, and the abdominal aorta was cut open, slowly infusing the normal saline solution through the jugular vein until the lung tissue became white. Then the whole lung was removed. The surface blood was rinsed with cold PBS, and the water on the surface of the tissue was absorbed by filter paper. After taking photos, the upper lobe of the left lung was weighed and homogenized with PBS (tissue mass [mg]/PBS volume [mL] = 0.07) on the ice by a homogenizer. The homogenate was transferred to a centrifuge for centrifugation (8000×*g*, 10 min, 4 °C). The supernatant was removed again (16000×*g*, 10 min, 4 °C), and the optical density value of the supernatant was measured at 590 nm using a full-wavelength enzyme label analyzer [D (590)], and the concentration of Evans Blue in the supernatant was obtained according to the standard curve of Evans Blue. The protein concentration of the supernatant was determined by BCA protein assay kit. Finally, the ratio of Evans blue mass to protein mass was used as the index of pulmonary vascular barrier.

6.Transendothelial electrical resistance (TER) and FITC-BSA leakage of Endothelial cells

TER and BSA leakage of endothelials were detected as previously described [12]. Primary endothelial cells were extracted as follow. Thoracotomy was performed under anesthesia with pentobarbital sodium solution (45 mg/kg intraperitoneal). Later the pulmonary vein in the left lung was exposed gently and subsequently took out, and the vein was washed for 4 times and cut to pieces, then the vein pieces were placed in the culture flask and cultured (DMEM-F12 medium, 10 % serum (Gibco, America). We have elaborated and explained this issue in the part of method. In brief, endothelials were seeded on the upper layer of Transwell (24-well, 0.4 μm, Coring, America), and pericytes were seeded on the opposite side. TER of endothelials was assessed by voltmeter (World Precision Inc, America), and the value of TER was recorded every 30 min. For the assessment of BSA leakage, FITC-BSA (10 μg/ml) was added into endothelials immediately after the treatment, and 200 μl supernatant of the lower insert of Transwell was collected and measured every 10 min, and 200 μl DMEM-F12 medium was supplemented into the upper insert to keep the balance of the culture system in Transwell.

7.Mitochondrial Oxygen Consumption Rate of pericytes

To measure the oxygen consumption rate (OCR), pericytes were seeded into a 24-well XFe plate (Seahorse, Agilent Cell Analysis Technology, USA) at a density of 2 × 104 cells per well. After seeding, the plates were placed on a clean bench and settled naturally for 1 h. The plate was incubated overnight to ensure proper cell adherence. Once the cells reached 70 % confluence, transfection of ACSL4-shRNA adenovirus and LPS treatment were initiated. Prior to the OCR detection, this study cultured pericytes in the basic medium containing 2.5 μM glucose and 2 mM glutamine for 50 min. Subsequently, pericytes were sequentially exposed to culture media containing 2 μM oligomycin, 2 μM FCCP, and 0.5 μM rotenone/antimycin A. Eventually, under mitochondrial stress conditions, this study utilized an extracellular flux analyzer to accurately determine the OCR of pericytes.

8.Transmission electron microscopy observation

The pulmonary venules were fixed in 3 % glutaraldehyde in 0.1 M PBS for 20 min, cut into blocks smaller than 1 mm3 and then immersion in the same fixative overnight at 4 °C. Samples were incubated in 1 % osmium tetroxide in 0.1 M PBS for 2 h at 4 °C, dehydrated, and then embedded in Epon 812. Ultrathin sections were stained with uranyl acetate and lead citrate. The ultrastructure of pulmonary venules was captured by transmission electron microscopy (H-7500; Hitachi, Japan).

9.Mitochondrial function assessment of pericytes

Pericytes were seeded into confocal dishes with a diameter of 20 mm. The adenovirus transfection treatment was the same as previously described. After another 12 h of LPS treatment, either JC-1 (10 μg/mL, 30 min at 37 °C) or MitoSox Red (5 μM, 10 min at 37 °C) was performed. Pericytes were detected via a laser confocal microscope ((Leica TCS SP5, Wetzlar, Germany). JC-1 monomer fluorescence was excited using a 488 nm laser, and emission was collected at 501–563 nm. MitoSOX and JC-1 aggregate fluorescence were excited using a 633 nm laser, with emission captured at 558–617 nm.

10. Detection of Lipid ROS and ferrous iron (Fe^{2+})

Pericytes were seeded into confocal dishes with a diameter of 20 mm

and treated as previously described. Either working solution BODIPY™ 581/591 C11 (10 μM, 30 min at 37 °C) or FerroOrange (1 μM, 30 min at 37 °C) was added. Oxidation of the polyunsaturated butadienyl part of the BODIPY™ 581/591 C11 causes the fluorescence emission peak to shift from ~590 nm to ~510 nm. In the reduced state, BODIPY™ 581/591 undecanoic acid has a maximum excitation and emission of 581/591 nm, respectively. In the oxidation state, the excitation and emission maxima were 488/510 nm, respectively. FerroOrange fluorescence were excited using a 561 nm laser, with emission captured at 570–620 nm.

11. Detection of organ function and blood gas

Blood (sodium citrate: blood = 1:9) was collected and centrifuged at 1500 g for 15 min to measure the cardiac function: cardiac troponin (TnT), liver function: aspartate aminotransferase (AST) and alanine aminotransferase (ALT), kidney function: blood urea nitrogen (Urea), and serum creatinine (Crea), by an automatic biochemistry analyzer in the clinical laboratory of Daping hospital. Blood gas was measured by a blood gas analyzer (ABL800).

12. Western blotting

Briefly, total proteins were extracted by RIPA buffer from cell samples or tissues samples, separated by SDS-PAGE and transferred to polyvinylidene fluoride membranes. After blocked by milk powder for 1 h, membranes were then incubated with primary antibodies at 4 °C overnight. β-actin was used as internal controls. The band intensity was analyzed using the Odyssey CLx Infrared Imaging System (LI-COR, Lincoln, NE, USA). The relative expression level of the target protein was calculated as the ratio of the target protein gray value to the internal reference gray value using ImageJ software (https://fiji.sc/). Antibodies are as follows: PDGFR-β (1:1000, ab32570, Abcam), NG-2 (1:1000, ab129051, Abcam), GPX4 (1:1000, ab125066, Abcam), COX2 (1:1000, ab179800, Abcam), YAP1 (1:1000, A1001, Abclonal), PGC-1α (1:1000, A12348, Abclonal) and β-actin (1:6000, ab8226, abcam).

13. Pericytes transfection

Pericytes were transfected with ACSL4-shRNA adenovirus, YAP1-shRNA adenovirus and GPX4-overexpressing adenovirus (Genechem Technology, China) according to experiments design. Corresponding adenovirus was co-incubated with pericytes in the presence of Opti-MEM when cells were 50–80 % confluence, by 60 MOI of the virus solution. Approximately 12h post-transfection, the culture medium containing the adenovirus was removed and fresh complete pericytes medium was added.

14. LC-MS/MS metabolomics

The metabolites were extracted using a 400 μL methanol: water (4:1, v/v) solution with 0.02 mg/mL L-2-chlorophenylalanin as internal standard. The mixture was treated by high throughput tissue crusher Wonbio-96c (Shanghai wanbo biotechnology co., LTD). After centrifugation, the supernatant was carefully transferred to sample vials for LC-MS/MS analysis. A pooled quality control sample (QC) was prepared by mixing equal volumes of all samples. The QC samples were disposed and tested in the same manner as the analytic samples. The instrument platform for LC-MS analysis is the ultra-high performance liquid chromatography tandem time-of-flight mass spectrometry UPLC-Triple TOF system of AB SCIEX. The raw data of LC/MS is preprocessed by Progenesis QI (Waters Corporation Milford, USA) software, and a three-dimensional data matrix in CSV format is exported. Perform variance analysis on the matrix file after data preprocessing. The R package ropls (Version 1.6.2) performed principal component analysis (PCA) and orthogonal least partial squares discriminant analysis (OPLS-DA), and used 7-cycle interactive validation to evaluate the stability of the model. In addition, student's t-test and fold difference analysis were performed. The selection of significantly different metabolites was determined based on the Variable importance in the projection (VIP) obtained by the OPLS-DA model and the p-value of student's *t*-test, and the metabolites with VIP>1, $p < 0.05$ were significantly different metabolites. Differential metabolites among two groups were summarized, and mapped into their biochemical pathways through metabolic enrichment and pathway analysis based on database search.

15. LC-MS/MS proteomics

Total proteins of pericytes were extracted following LPS challenge 24h and then underwent reductive alkylation and digestion. The peptides were vacuum dried, then resuspended with 0.1 % TFA. Samples were desalted with HLB, and vacuum dried. Peptide concentrations were determined by peptide quantification kit (Thermo, Cat.23275). One unit of TMT reagent were thawed and reconstituted in acetonitrile. After tagging for 2h at room temperature, hydroxylamine was added to react for 30 min at room temperature. Finally, all samples were pooled, desalted and vacuum-dried. The pooled samples were fractionated into fractions by Acquity Ultra Performance liquid chromatography (Waters, USA) with Acquity UPLC BEH C18 Column (1.7 μm, 2.1 mm × 150 mm, Waters, USA) to increase proteomic depth. Labeled peptides were were analyzed by online nano flow liquid chromatography tandem mass spectrometry performed on an Easy-nLC system (Thermo, USA) connected to a Q_Exactive HF-X (Thermo, USA) through a nanoelectrospray ion source. The RAW data files were analyzed using ProteomeDiscoverer (Thermo Scientific, Version 2.4). The thresholds of fold change (>1.2 or <0.83) and P-value <0.05 were used to identify differentially expressed proteins.

16. Construction of pericytes targeting liposomes

Soybean Lecithin, cholesterol, two targeted peptides, adenovirus and Cy5.5 were dissolved together in 3 mL chloroform and evaporated into a film under reduced pressure in the sample bottle. 2 mL of deionized water was added. It was treated with ultrasound and liposome extruder (polycarbonate membrane, pore size 200 nm). The unloaded polypeptides, adenoviruses and Cy5.5 were removed by dialysis apparatus (polycarbonate membrane, pore size 50 nm). Finally, the volume is fixed to 5 mL by adding deionized water. 10 μL liposome solution was added with 1 % Triton x-100 to determine the content of adenovirus in liposomes by ultraviolet spectrophotometer. Finally, liposomes were lyophilised and stored at 4 °C.

17. Detection of lipid ROS of pericytes in the lungs

Initially, we collected the upper lobe of the right lung tissues from rats, washed it with normal saline, and then placed it in serum-free 1640 medium. The lungs were placed in 3–5 mL of tissue digestion solutionI, cut with ophthalmic scissors and placed in 37 °C water bath for 30 min. During digestion, we blew tissues several times every 10 min to prevent accumulation. After filtration, the remaining tissues were digested with tissue digestion solution II at 37 °C for 30 min and then filtered. The liquid was transferred to a centrifuge for centrifugation (400×*g*, 5 min, 4 °C) and precipitation was collected. Then, red blood cell lysate was added.

Cells were divided into 1.5 ml EP tubes at 100 μl each for subsequent flow antibody staining, CD13 (PE, 1:20), CD31 (APC, 1:20), CD45 (BV510, 1:20). Cells were placed at room temperature and away from light for 30 min, then washed with cell stain buffer. Cells were centrifuged (400×*g*, 5 min, 4 °C), the precipitate was resuspended and the cells were incubated with BODIPY™ 581/591 C11 (10 μM, 30 min at 37 °C). Cells were centrifuged (400×*g*, 5 min, 4 °C), the precipitate was resuspended and the cells were incubated with DAPI (1:10000). The cells were left at room temperature and away from light for 5 min, and

the assay was carried out directly without washing.

18. Statistical analysis

All statistical analyses were performed using SPSS 20.0 (SPSS Inc., Chicago, IL, USA). The results are expressed as mean ± standard deviation for the indicated number of experiments. Independent sample t-tests were used for statistical analysis between two groups, and one-way analysis of variance (ANOVA) for comparisons involving more than two groups, followed by Tukey's post hoc test for pairwise comparisons. Survival data were analyzed using the log-rank test (Kaplan–Meier curves).

Statistical significance was set at $P < 0.05$.

Data availability

Data will be made available on request.

References

[1] M. Cecconi, L. Evans, M. Levy, A. Rhodes, Sepsis and septic shock, Lancet 392 (10141) (2018) 75–87.
[2] M. Singer, C.S. Deutschman, C.W. Seymour, et al., The Third international Consensus definitions for sepsis and septic shock (Sepsis-3), JAMA, J. Am. Med. Assoc. 315 (8) (2016) 801–810.
[3] C. Lelubre, J.L. Vincent, Mechanisms and treatment of organ failure in sepsis, Nat. Rev. Nephrol. 14 (7) (2018) 417–427.
[4] E. Siddall, M. Khatri, J. Radhakrishnan, Capillary leak syndrome: etiologies, pathophysiology, and management, Kidney Int. 92 (1) (2017) 37–46.
[5] A.C.P. Souza, P.S.T. Yuen, R.A. Star, Microparticles: markers and mediators of sepsis-induced microvascular dysfunction, immunosuppression, and AKI, Kidney Int. 87 (6) (2015) 1100–1108.
[6] D.A. Hartmann, V. Coelho-Santos, A.Y. Shih, Pericyte control of blood flow across microvascular zones in the central nervous system, Annu. Rev. Physiol. 84 (2022) 331–354.
[7] D. Attwell, A. Mishra, C.N. Hall, F.M. O'Farrell, T. Dalkara, What is a pericyte? J. Cerebr. Blood Flow Metabol. 36 (2) (2016) 451–455.
[8] A. Armulik, G. Genové, C. Betsholtz, Pericytes: developmental, physiological, and pathological perspectives, problems, and promises, Dev. Cell 21 (2) (2011) 193–215.
[9] J.J. Wang, J. Shen, Gut vascular barrier in the pathogenesis and resolution of Crohn's disease: a novel link from origination to therapy, Clin. Immunol. 253 (2023) 12.
[10] N.M. O'Brown, N.B. Patel, U. Hartmann, A.M. Klein, C.H. Gu, S.G. Megason, The secreted neuronal signal Spock1 promotes blood-brain barrier development, Dev. Cell 58 (17) (2023), 1534-+.
[11] Z.S. Zhang, Y.Y. Liu, S.S. He, et al., Pericytes protect rats and mice from sepsis-induced injuries by maintaining vascular reactivity and barrier function: implication of miRNAs and microvesicles, Military Med Res 10 (1) (2023) 17.
[12] H.N. Zhou, D.Y. Zheng, H.C. Wang, et al., The protective effects of pericyte-derived microvesicles on vascular endothelial functions via CTGF delivery in sepsis, Cell Commun. Signal. 19 (1) (2021) 20.
[13] S.S. He, Z.S. Zhang, X.Y. Peng, et al., The protective effect of pericytes on vascular permeability after hemorrhagic shock and their relationship with Cx43, Front. Physiol. 13 (2022) 16.
[14] H. Zeng, X.C. He, Q.H. Tuo, D.F. Liao, G.Q. Zhang, J.X. Chen, LPS causes pericyte loss and microvascular dysfunction via disruption of Sirt3/angiopoietins/Tie-2 and HIF-2α/Notch3 pathways, Sci. Rep. 6 (2016) 13.
[15] P.F. Li, Y. Zhou, A.J. Goodwin, et al., Fli-1 governs pericyte dysfunction in a murine model of sepsis, J. Infect. Dis. 218 (12) (2018) 1995–2005.
[16] P.F. Li, A.J. Goodwin, J.A. Cook, P.V. Halushka, X.K. Zhang, H.K. Fan, Fli-1 transcription factor regulates the expression of caspase-1 in lung pericytes, Mol. Immunol. 108 (2019) 1–7.
[17] P.F. Li, Y. Wu, E.D. Hamlett, et al., Suppression of Fli-1 protects against pericyte loss and cognitive deficits in Alzheimer's disease, Mol. Ther. 30 (4) (2022) 1451–1464. Li J, Cao F, Yin HL, Huang ZJ, Lin ZT, Mao N, Sun B, Wang G. Ferroptosis: past, present and future. Cell Death Dis. 2020 Feb 3;11(2):88.
[18] X. Jiang, B.R. Stockwell, M. Conrad, Ferroptosis: mechanisms, biology and role in disease, Nat. Rev. Mol. Cell Biol. 22 (4) (2021 Apr) 266–282.
[19] L. Xl, Z. Gy, G. R, C. N, Ferroptosis in sepsis: the mechanism, the role and the therapeutic potential, Front. Immunol. 13 (2022 Aug 5) 956361.
[20] C. Wang, W. Yuan, A. Hu, J. Lin, Z. Xia, C.F. Yang, Y. Li, Z. Zhang, Dexmedetomidine alleviated sepsis induced myocardial ferroptosis and septic heart injury, Mol. Med. Rep. 22 (1) (2020 Jul) 175–184.
[21] J. Wang, Q. Zhu, Y. Wang, J. Peng, L. Shao, X. Li, Irisin protects against sepsis-associated encephalopathy by suppressing ferroptosis via activation of the Nrf2/GPX4 signal axis, Free Radic. Biol. Med. 187 (2022 Jul) 171–184, https://doi.org/10.1016/j.freeradbiomed.2022.05.023. Epub 2022 Jun 1. Erratum in: Free Radic Biol Med. 2022 Nov 20;193(Pt 2):676.
[22] B. Jia, J. Li, Y. Song, C. Luo, ACSL4-Mediated ferroptosis and its potential role in central nervous system diseases and injuries, Int. J. Mol. Sci. 24 (12) (2023 Jun 12) 10021.
[23] F. Ursini, M. Maiorino, Lipid peroxidation and ferroptosis: the role of GSH and GPx4, Free Radic. Biol. Med. 152 (2020 May 20) 175–185.
[24] J. Wu, A.M. Minikes, M. Gao, H. Bian, Y. Li, B.R. Stockwell, Z.N. Chen, X. Jiang, Intercellular interaction dictates cancer cell ferroptosis via NF2-YAP signalling, Nature 572 (7769) (2019 Aug) 402–406.
[25] S. Magesh, D. Cai, Roles of YAP/TAZ in ferroptosis, Trends Cell Biol. 32 (9) (2022 Sep) 729–732.
[26] H. Huang, Pericyte-endothelial interactions in the retinal microvasculature, Int. J. Mol. Sci. 21 (19) (2020) 18.
[27] S. Ayloo, C.G. Lazo, S.H. Sun, W. Zhang, B.X. Cui, C.H. Gu, Pericyte-to-endothelial cell signaling via vitronectin-integrin regulates blood-CNS barrier, Neuron 110 (10) (2022), 1641-+.
[28] A.M. Nikolakopoulou, A. Montagne, K. Kisler, et al., Pericyte loss leads to circulatory failure and pleiotrophin depletion causing neuron loss, Nat. Neurosci. 22 (7) (2019) 1089–+.
[29] H.S. Shi, Y. Koronyo, A. Rentsendorj, et al., Identification of early pericyte loss and vascular amyloidosis in Alzheimer's disease retina, Acta Neuropathol. 139 (5) (2020) 813–836.
[30] E. Kang, J.W. Shin, Pericyte-targeting drug delivery and tissue engineering, Int. J. Nanomed. 11 (2016) 2397–2406.
[31] Y.Y. Guan, X. Luan, J.R. Xu, et al., Selective eradication of tumor vascular pericytes by peptide-conjugated nanoparticles for antiangiogenic therapy of melanoma lung metastasis, Biomaterials 35 (9) (2014) 3060–3070.
[32] F. Pastorino, C. Brignole, M. Loi, et al., Nanocarrier-mediated targeting of tumor and tumor vascular cells improves uptake and penetration of drugs into neuroblastoma, Front. Oncol. 3 (2013) 190.
[33] Y.Y. Zhang, B.T. Ning, Signaling pathways and intervention therapies in sepsis, Signal Transduct. Targeted Ther. 6 (1) (2021) 36.
[34] A. Mushtaq, F. Kazi, Updates in sepsis management, Lancet Infect. Dis. 22 (1) (2022) 24.
[35] P. Sinha, V.E. Kerchberger, A. Willmore, et al., Identifying molecular phenotypes in sepsis: an analysis of two prospective observational cohorts and secondary analysis of two randomised controlledtrials, Lancet Respir. Med. 11 (11) (2023) 965–974.
[36] S.V. Bhavani, M. Semler, E.T. Qian, et al., Development and validation of novel sepsis subphenotypes using trajectories of vital signs, Intensive Care Med. 48 (11) (2022) 1582–1592.
[37] Y. Jiao, T. Zhang, C.M. Zhang, et al., Exosomal miR-30d-5p of neutrophils induces M1 macrophage polarization and primes macrophage pyroptosis in sepsis-related acute lung injury, Crit. Care 25 (1) (2021) 15.
[38] J.F. Wang, Y.P. Wang, J. Xie, et al., Upregulated PD-L1 delays human neutrophil apoptosis and promotes lung injury in an experimental mouse model of sepsis, Blood 138 (9) (2021) 806–810.
[39] I. Park, M. Kim, K. Choe, et al., Neutrophils disturb pulmonary microcirculation in sepsis-induced acute lung injury, Eur. Respir. J. 53 (3) (2019) 14.
[40] W. Chen, C. Miao, et al., Neutrophil extracellular traps mediate m6A modification and regulates sepsis-associated acute lung injury by activating ferroptosis in alveolar epithelial cells, Int. J. Biol. Sci. 18 (8) (2022 May 9) 3337–3357.
[41] Y. Zhao, J. Ren, et al., The interaction between STING and NCOA4 exacerbates lethal sepsis by orchestrating ferroptosis and inflammatory responses in macrophages, Cell Death Dis. 13 (7) (2022 Jul 28) 653.
[42] G.T. Xu, J. Zhang, et al., Melatonin maintains inner blood-retinal barrier by regulating microglia via inhibition of PI3K/Akt/Stat3/NF-kappaB signaling pathways in experimental diabetic retinopathy, Front. Immunol. 13 (2022) 831660.
[43] H. X, H.Y. Kuang, et al., Autophagy modulates the migration of retinal pericytes induced by advanced glycation end products, Evid. Based Complement. Altern. Med. 2022 (2022) 2760537.
[44] F. Barutta, S. Bellini, G. Gruden, Mechanisms of podocyte injury and implications for diabetic nephropathy, Clin. Sci. 136 (2022) 493–520.
[45] A. Jiang, A. Song, C. Zhang, Modes of podocyte death in diabetic kidney disease: an update, J. Nephrol. 35 (2022) 1571–1584.
[46] M.D. Sweeney, A.P. Sagare, B.V. Zlokovic, Blood-brain barrier breakdown in Alzheimer disease and other neurodegenerative disorders, Nat. Rev. Neurol. 14 (2018) 133–150.
[47] B. Zingarelli, H. Fan, et al., Fli-1 governs pericyte dysfunction in a murine model of sepsis, J. Infect. Dis. 218 (2018) 1995–2005.
[48] G. Stallone, G. Castellano, et al., Double labeling of PDGFR-beta and alpha-SMA in swine models of acute kidney injury to detect pericyte-to-myofibroblast transdifferentation as early marker of fibrosis, Bio Protoc. 10 (2020) e3779.
[49] G. Wang, S. Xu, et al., Ferrostatin-1 alleviates lipopolysaccharide-induced acute lung injury via inhibiting ferroptosis, Cell. Mol. Biol. Lett. 25 (2020) 10.
[50] S. Hu, L. Zhu, et al., Electroacupuncture alleviates LPS-induced ARDS through alpha7 nicotinic acetylcholine receptor mediated inhibition of ferroptosis, Front. Immunol. 13 (2022) 832432.
[51] H. Meng, W. Lin, et al., Itaconate inhibits ferroptosis of macrophage via Nrf2 pathways against sepsis-induced acute lung injury, Cell Death Discovery 8 (1) (2022) 43.
[52] Y. Wang, M.H. Zhang, R. Bi, et al., ACSL4 deficiency confers protection against ferroptosis-mediated acute kidney injury, Redox Biol. 51 (2022) 13.
[53] P. Liao, W.M. Wang, W.C. Wang, et al., $CD8^+$ T cells and fatty acids orchestrate tumor ferroptosis and immunity via ACSL4, Cancer Cell 40 (4) (2022) 365–+.
[54] S. Doll, B. Proneth, Y.Y. Tyurina, et al., ACSL4 dictates ferroptosis sensitivity by shaping cellular lipid composition, Nat. Chem. Biol. 13 (1) (2017) 91–98.

[55] P. Willems, R. Rossignol, C.E.J. Dieteren, M.P. Murphy, W.J.H. Koopman, Redox homeostasis and mitochondrial dynamics, Cell Metabol. 22 (2) (2015) 207–218.
[56] J. Li, Y.C. Jia, Y.X. Ding, J. Bai, F. Cao, F. Li, The crosstalk between ferroptosis and mitochondrial dynamic regulatory networks, Int. J. Biol. Sci. 19 (9) (2023) 2756–2771.
[57] N. Ta, C. Qu, H. Wu, et al., Mitochondrial outer membrane protein FUNDC2 promotes ferroptosis and contributes to doxorubicin-induced cardiomyopathy, Proc. Natl. Acad. Sci. U. S. A. 119 (36) (2022) 12.